agronomy

MDPI

Article

Precision Turfgrass Irrigation: Capturing Spatial Soil Moisture Patterns with ECa and Drone Data

Ruth Kerry [1,*], Ben Ingram [2], Kirsten Sanders [1], Abigail Henrie [1], Keegan Hammond [3], Dave Hawks [4], Neil Hansen [3], Ryan Jensen [1] and Bryan Hopkins [3]

[1] Geography Department, Brigham Young University, Provo, UT 84602, USA
[2] School of Water, Energy and Environment, Cranfield University, Cranfield MK43 0AL, Bedfordshire, UK
[3] Plant and Wildlife Science Department, Brigham Young University, Provo, UT 84602, USA
[4] Physical Facilities Site Development, Brigham Young University, Provo, UT 84602, USA
* Correspondence: ruth_kerry@byu.edu

Abstract: Turfgrass irrigation consumes a large amount of the scarce freshwater in arid/semi-arid regions. Approximately 50% of this irrigation water is wasted. It has been suggested that determining patterns of spatial variability in soil moisture to modify applications with valve-in-head sprinkler technology can greatly reduce waste. Variable rate irrigation (VRI) studies in traditional agricultural settings have shown that VRI zones do not stay static temporally and need to be frequently redetermined. Electrical conductivity (ECa) data from Geonics EM38 surveys and data from Red, Green, Blue (RGB) and Thermal Infra-Red (Th.IR) drone surveys are less time-consuming and therefore expensive to collect than a dense field survey of soil moisture and grass health to produce accurate geostatistical maps. Drone flights and ECa surveys are compared here for their ability to accurately estimate spatial patterns of soil volumetric water content (VWC) using simple linear regression and z-score transformations for prediction—non-geostatistical approaches that require less data. Overall, ECa readings collected in the horizontal mode were the most consistent at capturing spatial patterns in soil moisture. Predictions from regression produced lower root mean squared errors (RMSEs) for the larger datasets. However, z-score transformation produced lower RMSEs when the sample number was very small and preserved the scale of values better than the regression approach. The results suggested that predictions from ECa and drone data were useful for capturing key features in soil moisture patterns for 2–3 weeks, suggesting that a periodic reassessment of zones is needed. Using ECa and drone data in an urban environment is more labor-intensive than in an agricultural field, so it is likely that automating periodic re-surveying of ECa data for zone definition would only be cost-effective for golf courses or high-income sports fields. Elsewhere, using static zones with variable rates applied to each zone may be more efficient.

Keywords: soil mapping; management zones; variable rate irrigation (VRI); sensed data

Citation: Kerry, R.; Ingram, B.; Sanders, K.; Henrie, A.; Hammond, K.; Hawks, D.; Hansen, N.; Jensen, R.; Hopkins, B. Precision Turfgrass Irrigation: Capturing Spatial Soil Moisture Patterns with ECa and Drone Data. *Agronomy* **2024**, *14*, 1238. https://doi.org/10.3390/agronomy14061238

Academic Editors: Tiago Brito Ramos, Yanbo Huang and Hanaa Darouich

Received: 6 May 2024
Revised: 1 June 2024
Accepted: 5 June 2024
Published: 7 June 2024

1. Introduction

Megadroughts are defined as droughts lasting decades or even centuries [1]. The American Mountain West has been experiencing a "megadrought" in the 21st century [2]. Williams et al. [3] noted that the severe and persistent 21st-century drought in southwestern North America was exceeded only by a late-1500s megadrought. Evidence of the current megadrought in the west was shown in May 2021 by http://droughtmonitor.unl.edu (accessed on 31 May 2021), whereby 30% of the west was experiencing extreme or exceptional drought. In the state of Utah, megadrought has been evidenced by the shrinking of the Great Salt Lake by 50–60% between 1985 and 2022 [4], but the shrinking of the Great Salt Lake is also evidence of an increase in human water use in the region [5], particularly by agriculture [6] and in urban areas. According to the 2020 US Census, Utah was the fastest-growing state in the USA with a gain of 507,731 residents, with 35% of that increase

coming from net migration [7]. In addition, 90% of the expanding Utah population lives in urban areas [8]. This urban population expansion, in conjunction with the megadrought, has put stress on the limited freshwater resources.

In Utah and in some other semi-arid areas around the USA and the world, most residences and institutions have irrigated turfgrass. With increased urbanization in the USA, Milesi et al. noted in 2005 [9] that there were more irrigated acres of turfgrass than irrigated corn, wheat and fruit trees combined. The figures from this study are still being quoted nearly 20 years on but no new evaluations of this situation have been provided, only suggestions that the Milesi et al. [9] study overestimated the amount of irrigated turfgrass, as they assumed that the total acreage of turfgrass grown in the USA was irrigated [10]. Nevertheless, as 25% of the continental USA is semi-arid or arid [11], turfgrass in these areas will be frequently irrigated as is turfgrass in areas with less extreme climates. Turfgrass has several advantages in urban areas, such as cooling [12], carbon fixation [13,14], cleaning noxious gases from the air [15] and reduction in fire risk [16], but when irrigated, it uses a large amount of scarce freshwater.

Traditionally, sports field managers have carried out periodic site assessments of soil and turfgrass characteristics in four to six sample areas per field. Precision turfgrass management is a relatively new approach in turfgrass management [17–19] which considers more detailed spatial variation in grass health, nutrients, compaction and soil moisture to determine where fertilizer, herbicide and water are needed and where they are not needed. This approach has developed drawing on the principles of precision agriculture, which has been practiced since the 1990s [18]. The aim of precision agriculture is to maximize profits and minimize adverse environmental effects [20]. Precision irrigation, or variable rate irrigation, is a key part of precision turfgrass management particularly in arid or semi-arid areas and could result in more efficient use of limited freshwater resources.

Between 30 and 60% of urban freshwater is used on lawns in the USA [21] and the United States Environmental Protection Agency (EPA) has estimated that about 50% of turfgrass irrigation water is wasted by temporal and spatial misapplications, with the latter accounting for larger proportions of waste [12]. This is a general figure and it is assumed that less water is wasted by trained sports field managers than uneducated residential lawn owners. Temporal misapplication of irrigation water can be reduced by the use of smart sprinkler systems, which consider local weather conditions in the scheduling of irrigation [22–28]. Precision turfgrass irrigation could also employ soil moisture sensors in existing sprinkler zones to determine when to apply water. With "valve-in-head" sprinkler technology, the rate of application can be varied from each individual sprinkler head rather than for a group of sprinkler heads, which form a zone for traditional sprinkler head technology. Developing spatial zones to be used with "valve-in-head" sprinkler technology, or determining different rates of irrigation that should be applied to existing sprinkler zones, is key to addressing spatial misapplications. Such variable rate irrigation is an important part of precision turfgrass management.

The first step in VRI is to characterize the spatial variation in soil moisture either directly through measurement with handheld devices [29,30] or through sensing-related properties through proximal [19,31,32] or remote sensing [33,34]. Within the discipline of precision agriculture, grid sampling at a suitable intensity followed by kriging has been shown to produce accurate maps of key soil properties [35]. However, the sampling interval used for the grid should be selected to resolve the variation at a suitable scale for field management and about 100 samples are required to compute accurate variograms for kriging [36]. Indeed, in turfgrass studies, data have been collected at 80–150 points in turfgrass sports fields using handheld devices [29,30,37]. This density of data collection is necessary to produce accurate maps by kriging. While handheld devices are not particularly expensive, gathering data on several variables at once on a dense grid with about 100 locations can take a few hours. Within precision agriculture, various sensing approaches have been embraced [38]. Sensors are generally more expensive than handheld devices, but far more dense datasets can be collected in a fraction of the time needed for a

dense survey with handheld devices. Indeed, a mobile multi-sensor platform that measures the VWC, penetrometer resistance, NDVI and GPS location all at once has been used in turfgrass fields and has been shown to be efficient in terms of sampling time and effort to obtain a very dense survey of fields [19,32,39].

Most research related to precision management (nutrients and irrigation) of turfgrass or VRI has been confined to maintaining turfgrass quality for golf courses or high-income sports fields while using less water [31,40–45]. This is primarily because the cost of mapping or sensing soil moisture levels can be somewhat offset by the income derived from the sporting activities that occur on these fields. However, for general sports fields, parks, recreation areas and suburban residential lawns, there is little or no income from crops or sporting activities that could pay for soil moisture mapping for the development of spatial zones. Also, residential customers are risk-averse and are much more likely to be willing to buy a smart sprinkler controller than make the significant investment of converting their irrigation infrastructure to valve-in-head technology or replanting their lawn to a low-input turfgrass [46,47]. Therefore, relatively less expensive means of mapping spatial patterns in soil moisture need to be found, especially those that could be somewhat automated

Another potential challenge with mapping spatial soil moisture zones for turfgrass is that within agriculture, it has been shown that temporally variable irrigation zones may be needed, because zones do not stay static once variable management practices are used [25]. Indeed, zones may need reassessment before each irrigation event. A University of Georgia group addressed this issue with sensor networks [44] and a USDA-ARS team in Bushland, TX, attached IR thermometers to central irrigation pivots to track canopy temperatures to calculate crop water stress in cotton [25]. Similarly, in the context of turfgrass, Straw and Henry [48] investigated two natural turfgrass sports fields and showed that during a dry down period, zones based on the volumetric water content (VWC), normalized difference vegetation index (NDVI) and penetration resistance changed, so the change in zones over time needs to be investigated. However, in contrast, it was shown that for turfgrass, a single irrigation event did not noticeably change the strength of relationships between or spatial distributions of field properties [49].

Kerry et al. [37] investigated the abilities of various costly and inexpensive field survey methods to reproduce patterns of soil moisture. Some of the methods were based on human perception [50]; however, of the methods investigated, none could be automated and none would be economically sustainable for the repeated mapping of soil moisture. However, sports field and golf course managers have a significant knowledge of how turfgrass health and soil moisture vary just from being familiar with their fields [51]. This knowledge could be used for an initial zoning and in situ sensors at minimal locations could be used to inform irrigation scheduling. The utility of field manager knowledge needs to be investigated further in the future.

In this paper, the issue of whether temporally varying VRI zones for turfgrass can be determined accurately and more swiftly with electrical conductivity (ECa) and drone data is addressed. ECa data collected using the Geonics EM38 instrument (Geonics Limited, Mississauga, ON, Canada) pulled behind a quad bike have been used to infer variations in soil moisture and nutrients for some time in precision agriculture [52–54]. The ability of soil to conduct electricity is related to its moisture content, which is in turn related to the soil's texture, compaction and nutrient content. Similarly, reflectance information from different wavelengths collected by satellite, plane or drone have been used in precision agriculture for detecting spatial variation in soil properties for defining fertilization and irrigation zones relatively inexpensively [55,56]. Most notable is the use of thermal waveband images (Th.IR) for mapping crop water stress for irrigation zoning and scheduling [57–60]. Data from the EM38 instrument and drones can be collected on-the-go and this is generally less labor-intensive than using handheld devices to conduct dense field surveys for geostatistical mapping [61], like that of Kerry et al. [37]. Drone and ECa surveys take about 30 min in contrast to 1–3 h for a dense field survey with handheld devices. However, neither ECa

collection [62] nor capture of information by drone [33,34] have been extensively used in the context of precision irrigation of turfgrass.

Sensed information usually offers a far denser dataset than can be efficiently collected on the ground through sampling or handheld sensors. Within precision agriculture, methods have been sought to use a combination of sampled soil data and sensed data in the mapping process to obtain accurate maps more cheaply. Such approaches capitalize on the density of the sensed data and the correct range of values of the sample data. In reviewing approaches for mapping soil properties using sensed information in precision agriculture, Adamchuk et al. [63] noted that usually, some ground truth data on the properties themselves need to be collected to calibrate the sensed data. Traditional field sampling and lab analysis is expensive, and the cost is proportional to the sample size [64]; therefore, it is desirable to use the smallest sample size that gives the best estimates. Similarly, the time taken to conduct grid surveys of turfgrass health and soil properties varies with sample size [29,30]. The sample sizes discussed in the case studies presented by Adamchuk et al. [63] were for mapping soil nutrients, physical properties and organic matter levels in agricultural fields, in conjunction with sensed data, but ranged from 10 to 75 samples and were usually based on a regression approach for calibration. Kerry et al. [65] investigated the use of an approach calibrating z-scores of sensed data with the means and standard deviations of samples of different sizes (12-296). They found that estimates of management zone averages [64] based on a z-score calibration were most accurate for the smallest sample sizes [65]. Given that there is no crop to offset the price of sensing for turfgrass, the sample size for calibration should be as small as possible. Therefore, the z-score calibration and regression-based calibration with different sample sizes will be compared in this study.

Data from several dense field surveys (more time-consuming) of soil volumetric water content (VWC), ECa surveys and drone flights (less time-consuming) in the visible and Th.IR wavelengths collected in the summer of 2022 were used to investigate which data were more useful in determining temporally varying zones for urban turfgrass within season. The relative errors associated with both approaches were used in comparison to kriged data from the dense field surveys. The errors associated with increasing periods of time between the VWC survey and ECa or drone survey and decreasing numbers of soil ground data points for calibration were also assessed. A simple linear regression and z-score calibration approach for calibrating the ECa and drone data to give VWC data were also compared. This paper significantly expands on the initial study of Kerry et al. [66] by looking at information from several more temporal surveys of two of the fields and more detailed examination of the differences between prediction approaches.

2. Materials and Methods

2.1. Field Methods

Three general use sports fields with Kentucky bluegrass (*Poa pratensis* L.) on Brigham Young University campus in Provo, UT, USA, were assessed. This species is the most commonly seeded grass and is the predominate sports field turfgrass in northern climates, such as in Utah. It is a C-3 cool season species with excellent surface stability and cold hardiness [67]. The West Stadium (40.2575° N, 111.659° W), Harmon (40.256° N, 111.644° W) and MTC fields (40.262° N, 111.644° W) were surveyed on 20 m, 15 m and 20 m grids, respectively (Figure 1a–c). The topsoil VWC (%) (0–10 cm depth) was determined at grid points using the average of two measurements within 1 m of grid nodes using an ML3 Theta Probe (Delta-T Devices, Cambridge, UK). Although most grass roots occur between 10 and 15 cm depth, theta probes are often used for quick assessments of topsoil moisture in turfgrass. The soil texture for the field sites ranged from silty clay loam to sandy loam and, thus, the spatial VWC assessment was calibrated based on a "loam" soil texture. The VWC surveys of each field used in this study were performed on the following dates: West Stadium, 24 May 2022; Harmon, 26 April 2022, 4 May 2022 and 6 October 2022; and MTC field, 7 April 2022, 5 May 2022 and 5 October 2022.

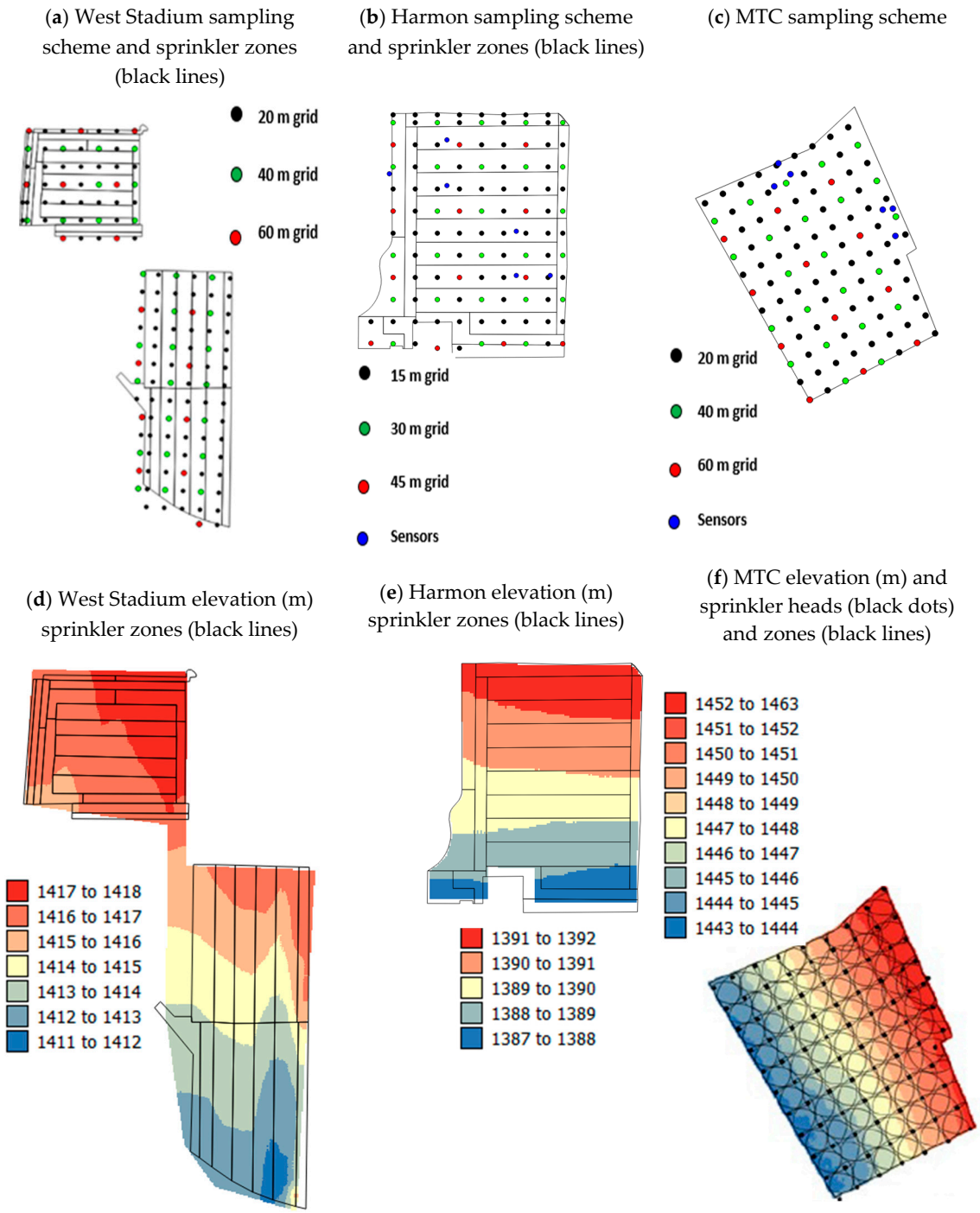

Figure 1. Sampling schemes and elevations (m above sea level) in relation to sprinkler zones, respectively, for the (**a**,**d**) West Stadium, (**b**,**e**) Harmon and (**c**,**f**) MTC fields.

The 15 m and 20 m grids used in each field for sampling the soil and grass were laid out using tape measures aligned with cardinal directions, as the accuracy of our Bad-Elf GNSS surveyor with 1 m accuracy was compromised to about 3 m accuracy by the proximity of the fields to tall buildings. These grid sizes were chosen so that the densest sampling would include 100–150 samples, as suggested is appropriate for geostatistical mapping by Webster and Oliver [36]. This allowed a dense, accurate mapping of the VWC for comparison with predicted values from regression and z-score transformation with smaller datasets. The dense 15 m and 20 m grid data were sub-sampled to make grids with double and triple the original sampling intervals (30 m and 45 m grids for the 15 m data and 40 m and 60 m

grids for the 20 m data) (Figure 1a–c). Additionally, in situ soil moisture sensors (Teros 12; Meter Group, Pullman, WA, USA) were installed for the Harmon and MTC fields at the locations shown in blue in Figure 1b,c. The soil sensor locations were determined based on previous soil moisture mapping within the fields. Locations were chosen to represent a range of relatively wet and dry locations but the wettest and driest locations were avoided. The numbers of samples for the different-sized grids in the West Stadium field were the following: 20 m = 135 points, 40 m = 34 points and 60 m = 17 points. For the Harmon field they were the following: 15 m = 101 points, 30 m = 30 points, 45 m = 13 points and sensor locations = 6 points. For the MTC field, the spacing and number of grid points were the following: 20 m = 103 points, 40 m = 27 points, 60 m = 12 points and sensor locations = 6 points.

Figure 1d–f show the orientation of sprinkler zones in relation to elevation patterns for the West Stadium, Harmon and MTC fields, respectively. For the West Stadium field, there was considerable variation in elevation within sprinkler zones as the zones were orientated in the opposite direction to elevation (Figure 1d). Although many of the soils under turfgrass fields on the university campus had been engineered to some extent, the West Stadium field showed no variation in the native soil type and had Keigley silty loam soils with 1–3% slopes throughout according to https://websoilsurvey.sc.egov.usda.gov/App/WebSoilSurvey.aspx (accessed 1 March 2024). The majority of sprinkler zones in the Harmon field were orientated with elevation (Figure 1e). The Harmon field had three native soil types: Taylorsville silty clay loam with 1 to 3% slopes (91.5% of the field), Pleasant Grove gravelly loam with 3 to 6% slopes (5.5% of the field), and Sterling gravelly fine sandy loam with 1 to 3% slopes (3% of the field) according to https://websoilsurvey.sc.egov.usda.gov/App/WebSoilSurvey.aspx (accessed 1 March 2024). We consider that the influence of the native soil identified by the web soil survey would be minimal in an engineered soil, but greater in the sub-soil. However, previous comparison tests of soil moisture from two different surveys showed highly significant differences in VWC ($p < 0.001$) between the three soil types identified by the web soil survey for the Harmon field. Also, the soil types with the highest and lowest VWCs were consistent between surveys. Finally, in the MTC field, "valve-in-head" sprinklers were installed so that each sprinkler head consisted of its own zone with a radius of 27 m, but the sprinkler heads themselves were spaced 20 m apart so there was overlap (Figure 1f) between the areas watered by each sprinkler head. The MTC field sprinkler heads were installed in the NW–SE running lines consistent with changes in elevation running across the slope (Figure 1f).

The MTC field had native soil of only one type, while the Pleasant Grove gravelly loam had 3 to 6% slopes according to https://websoilsurvey.sc.egov.usda.gov/App/WebSoilSurvey.aspx (accessed 1 March 2024). There was likely to be more difference in soil type within the MTC field than was identified by the web soil survey as this field had been dug up several times to insert pipelines, etc., along the main road. Also, a survey of topsoil texture along two NW–SE running transects showed soil textures varying between clay loam, loam and sandy loam [37], which is consistent with pipelines being installed beneath this field and the removed soil being replaced by sand. It was also consistent with the soils under turfgrass fields on the university campus being altered/engineered to some extent.

During the month of May 2022, A Geonics EM38 meter (Geonics Ltd., Mississauga, ON, Canada) was calibrated and then pulled across each field on a plastic sled in the horizontal and vertical positions to measure the Eca. The dates of the Eca survey for each field were the following: West Stadium field, 24 May 2022; Harmon field, 6, 9, 13, 17 23, 27 and 30 May 2022; and MTC field, 9, 13, 17, 23, 27 and 30 May 2022. The sled was pulled by a person or a slowly driven quad bike in the horizontal (Hz) and vertical (Vt) positions, with the average depths of inquiry being 0.75 m and 1.5 m, respectively [68]. Measurements were made once per second along transects spaced 5–10 m apart in each field (see tracks in black in Figure 2a,b,d). This transect spacing is consistent with the recommendation of 4.8–9.6 m being a desirable distance between transects for the Toro Precision Sense PS6000 multi-sensor platform [39].

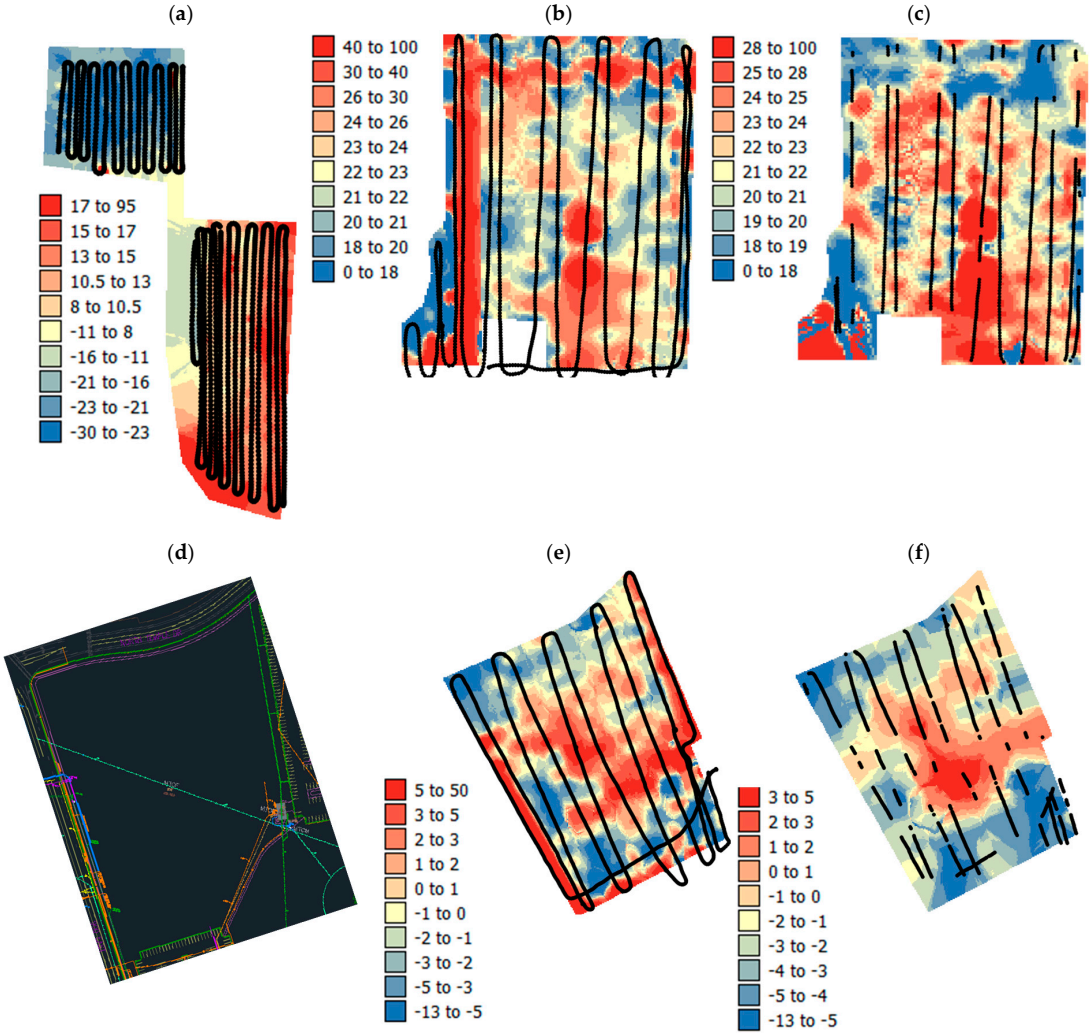

Figure 2. Maps showing how ECa data were preprocessed to remove highly conductive points. (**a**) Map of kriged raw HzEC and sample locations (black dots) in West Stadium field on 24 May. (**b**) Map of kriged raw HzEC and sample locations (black dots) in Harmon field on 9 May. (**c**) Map of kriged filtered HzEC and filtered sample locations (black dots) in Harmon field on 9 May. (**d**) Location of pipes and conductive features in MTC field. (**e**) Map of kriged raw ECa Vt values and sample locations (black dots) for MTC field on 13 May. (**f**) Map of kriged filtered ECa Vt values and filtered sample locations (black dots) for MTC field on 13 May.

In contrast to an agricultural environment where EM38 is often used as part of precision agricultural practices to indicate different zones in soil, there are many conductive features in an urban environment that influence ECa survey values. The locations of conductive features that might affect ECa measurements such as pipes, lampposts, drains and fences around and beneath the fields were mapped using the Global Navigation Satellite System (GNSS) and extracted from public or institutional record maps (Figure 2d). A 5 m buffer was applied to either side of known conductive points or features to filter out high values and points with an ECa > 3 standard deviations above the mean were also removed. The black dots in Figure 2c,f show the remaining ECa survey points after filtering. As Figure 2c,f show that some survey lines were removed completely by the filtering process, it is recommended that in an urban environment, to obtain a sufficient density of observations, practitioners should try to space transects at around 4.8 m rather than the 9.6 m top end of the recommended range of transect spacings [39].

Following ECa filtering, the data were kriged to create a raster with 1 m × 1 m pixels. There was also a problem with calibrating the EM38 instrument in locations that were

affected by unknown conductive features that were invisible at the surface and resulted in some negative ECa values that were still present after data filtering, as shown in Figure 2f. Therefore, exact HzEC and VtEC values could not be used to infer the VWC using existing pedotransfer functions. Rather, HzEC and VtEC values were used to infer spatial patterns in the ECa.

Th.IR and RGB drone surveys were performed for the fields using a Da-Jiang Innovations (DJI) Mavic 2 Enterprise (Da-Jiang Innovations, Shenzhen, China) drone at 61 m above ground level with a ground pixel size of ~6 cm. The thermal camera has an uncooled VOx microbolometer sensor with a 640 × 480 array capable of measuring temperatures between −10 °C and 140 °C. The RGB camera captures 12 mp images (4056 × 3040). Drone surveys for each field were performed on the following dates: West Stadium field, 24 May 2022; Harmon field, 8 April 2022, 5 October and 12 October 2022; MTC field, 8 April 2022, 19 May 2022, 5 and 12 October 2022. Images for each date and field were stitched together in Drone Deploy software online (dronedeploy.com) to make an ortho-mosaic as shown in the examples for West Stadium field in Figure 4d,e. Ground control points were used to check the locational accuracy of the orthomosaic. As the near infrared band was not captured by either camera on the drone, a vegetation index that used only visible wavebands was used. The visible atmospherically resistant index (VARI) was calculated from the individual wavebands using Equation (1) to give an indication of turfgrass health [69]:

$$VARI = \frac{Green - Red}{Green + Red - Blue} \quad (1)$$

2.2. Numerical Analysis

Figure 3 summarizes the steps involved in the data collection, processing, calibration and analysis that were used in this study. Grid-sampled soil VWC data were kriged to a 1 m grid using the software SpaceStat version 4.0.21 [70]. The ECa sample data were filtered as mentioned above and kriged to a 1 m grid. Drone data digital numbers (DNs) were degraded to give average values for a 1 m pixel size. To assess the degree of correlation between the VWC and the ECa and drone data from different dates, Pearson correlation coefficients were calculated between these variables using the data on the 1 m grid for each field in SPSS version 28 [71]. As correlation coefficients were computed between the 1 m kriged VWC estimates and the sensed data on a 1 m grid, $n > 13{,}000$ for each field site. Therefore, very low correlation coefficients were likely to be significant. Also, the significance of the correlation coefficients could have been overestimated due to spatial autocorrelation in the data [72] and therefore the relative strength of the correlations was most important in this study.

ECa and drone data were calibrated to give VWC values in two ways using the full survey data, sub-samples and sensor locations. First, the local average ECa and drone survey values were determined for each of the sub-sample points and sensor locations. The local averages were taken from the nearest 48 points on a 1 m kriging grid which is equivalent to 3rd-order queen neighbors or a search radius of 3 m. The local average ECa and drone values were then used with the VWC survey data to compute a regression model with the VWC as the dependent variable. The regression equation was used with the kriged ECa and drone survey data to estimate the VWC for the 1 m grid (regression calibration). The second calibration method (z-score calibration) involved converting the ECa and drone data to z-scores by subtracting the mean and dividing by the standard deviation of the ECa or drone data. The mean and the standard deviation of the VWC for each sub-sample (Figure 1a–c) were calculated. The ECa or drone z-scores were then multiplied by the standard deviation of the VWC measurements for the sub-sample and sensor locations and then the mean VWC for the given sub-sample was added (see Equations (1) and (2) of Kerry et al. [66] for further clarification). The kriged 1 m VWC data were used to compute root mean squared errors (RMSEs) between field-based dense VWC measurements that had been kriged and regression- and z-score-calibrated VWCs from the drone and ECa surveys.

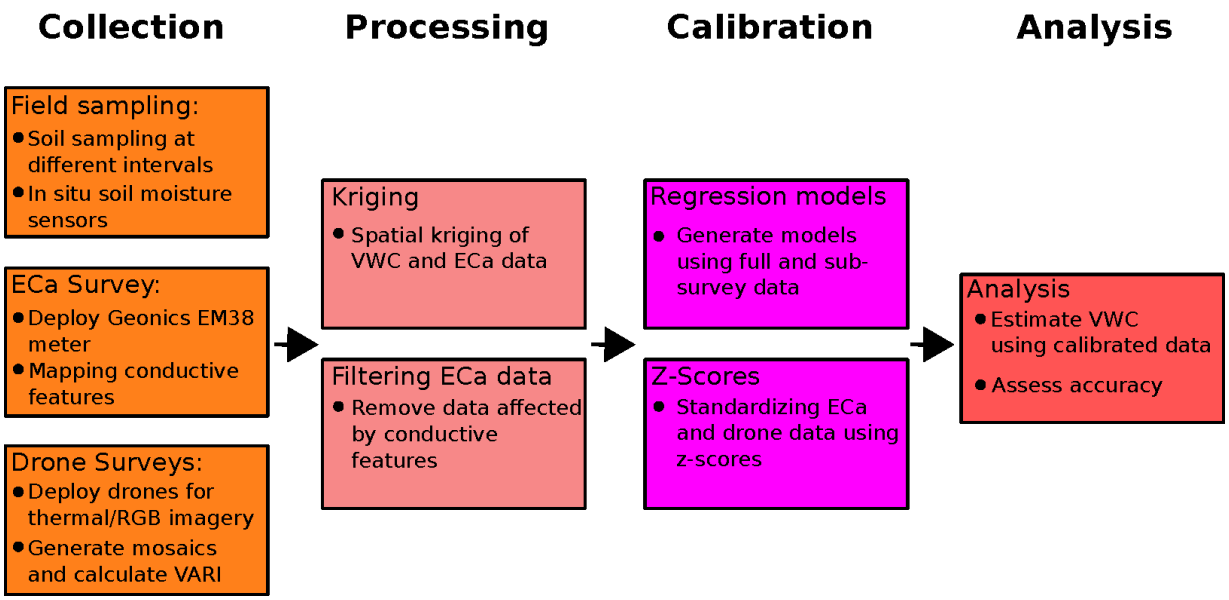

Figure 3. Flow chart summarizing the steps involved in the data collection, processing, calibration and analysis in this study.

3. Results and Discussion

3.1. West Stadium Field

3.1.1. Spatial Patterns in Variables

Figure 4 shows the VWC, HzEC, VtEC, Th.IR and VARI maps for the West Stadium field. All data were collected on 24 May 2022, so for this field, it was possible to investigate the relative errors involved in using ECa and drone data for prediction when they were collected on the same day as the VWC data. The maps show that there are similarities in the spatial patterns of these variables with VWC patterns. HzEC shows a strong positive relationship with the VWC (r = 0.75), while the VtEC, Th.IR and VARI show weaker negative relationships (r = −0.29, −0.20 and −0.25, respectively). The similarities between methods may in part be due to strong differences between the north and south parts of the field as no irrigation had occurred in the north in 2022.

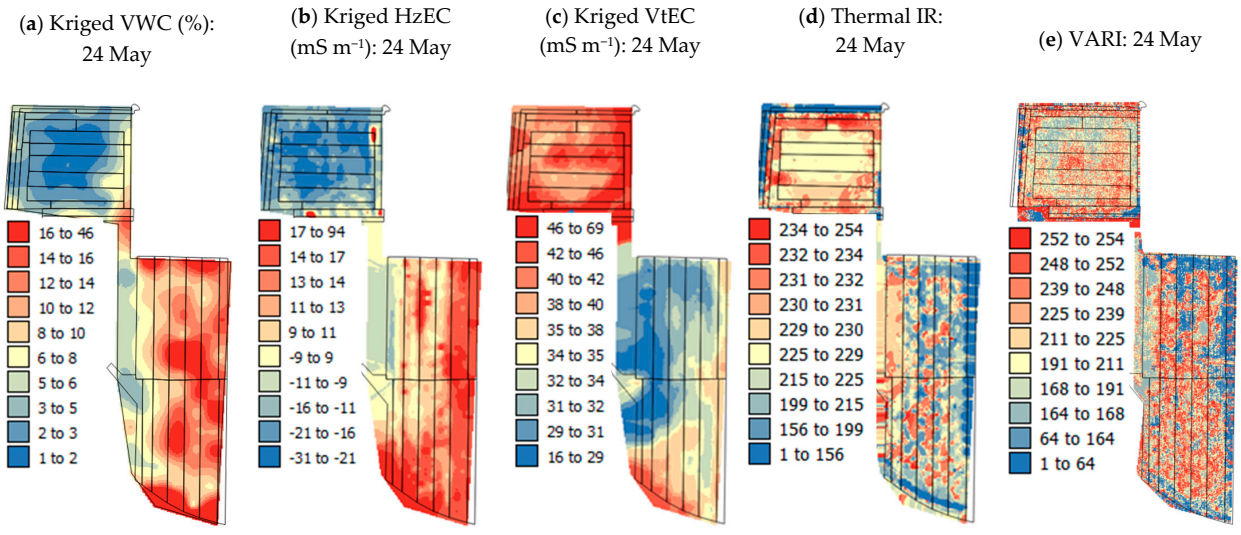

Figure 4. Kriged maps of the West Stadium field on 24 May 2022 for the (**a**) VWC, (**b**) HzEC, (**c**) VtEC, (**d**) thermal IR data and (**e**) VARI from 24 May 2022.

3.1.2. RMSEs for EC and Drone Data

Table 1 shows the RMSEs for the West Stadium field and shows that they are lower for the regression calibrations for all sample sizes. The RMSEs increase as sub-sampling interval increases and sample size decreases, showing that calibrations are more reliable when more field data are used. However, the increase in RMSEs is not proportionate to the decrease in sample size as the 20 m, 40 m and 60 m sub-samples contained 135, 34 and 17 samples, respectively. In the case of z-score calibration, RMSEs were notably larger across all variables and sampling grids. RMSEs were larger for VtEC, Th.IR and VARI than HzEC, showing that the HzEC data relate to the VWC at shallower depths [68] and are more suitable for characterizing spatial variation in topsoil VWC at this site than the other variables. As the HzEC gives information on shallower soil than the VtEC, and topsoil VWC (0–10 cm) is being used as a reference here, it is logical that the HzEC had lower RMSEs.

Table 1. Summary statistics and RMSEs for the VWC predicted using EC and drone data calibrated using regression and z-scores for the West Stadium field.

Data and Collection Date in 2022 (Month and Day)	Regression Calibration					z-Score Calibration				
	Min.	Max.	Mean	St. Dev.	RMSE	RMSE	Min.	Max.	Mean	St. Dev.
VWC 24 May 2022	1.47	45.84	8.98	6.04	–	–	1.47	45.84	8.98	6.04
HzEC 24 May 20 m	0.68	36.72	9.31	4.94	**4.07**	5.23	−4.05	52.76	9.56	7.89
HzEC 24 May 40 m	0.54	34.76	8.73	4.69	**4.04**	4.77	−3.39	48.13	8.95	7.06
HzEC 24 May 60 m	0.29	45.76	11.18	6.23	**4.91**	7.25	−8.18	67.91	10.04	10.04
VtEC 24 May 20 m	2.60	14.12	9.65	1.49	**5.83**	11.18	−13.86	46.52	9.56	7.79
VtEC 24 May 40 m	4.46	11.94	9.04	0.96	**5.84**	10.55	−12.29	42.47	8.95	7.06
VtEC 24 May 60 m	0.71	17.01	10.68	2.10	**6.04**	13.54	−21.33	59.55	10.04	10.43
Th.IR 24 May 20 m	9.39	10.10	9.53	0.15	**6.04**	10.78	−21.03	16.54	9.56	7.79
Th.IR 24 May 40 m	7.64	9.24	8.94	0.33	**6.12**	10.17	−18.79	15.28	8.95	7.06
Th.IR 24 May 60 m	3.82	12.34	10.76	1.77	**6.86**	13.10	−30.94	19.39	10.04	10.43
VARI 24 May 20 m	6.40	18.84	9.47	3.50	**6.21**	10.99	−11.28	16.37	9.56	7.79
VARI 24 May 40 m	5.44	20.14	9.06	4.14	**6.43**	10.36	−9.95	15.13	8.95	7.06
VARI 24 May 60 m	3.12	37.07	11.48	9.56	**10.28**	13.32	−17.88	19.17	10.04	10.43

Key: Th.IR = thermal infra-red, VARI = VARI index, HzEC = electrical conductivity horizontal mode, VtEC = electrical conductivity vertical model. **Bold** values show the lowest RMSEs for a given variable, sample size and date.

Table 1 also shows the minimum, maximum and mean of the calibrated VWC values for each sub-sample and variable compared to the measured VWC values. The calibrated values show that the mean was reasonably reproduced by both calibration methods and to the least extent for the least dense 60 m data. The range of values, particularly the maximum values, was severely reduced for the regression calibration, especially for the VtEC, TH, IR and VARI data. The z-score calibration also has low maximum values for the VWC predictions but has a greater range of values as the minimum values are all negative. While a calibration method should be able to produce low errors overall, if this is performed by effectively estimating the mean VWC but not capturing the true range of variation, this can be a problem. The HzEC data were the best for estimating the VWC within this field as the mean and range of predictions were closer to those of the measured VWC data for both calibration methods.

Figure 5 shows the VWC values predicted using the HzEC (the best-performing variable based on RMSEs), the regression and z-score calibrations, and the different-sized sub-samples. All maps (Figure 5) are plotted to the same numerical scale as the VWC surveyed in the field (Figure 4a). When the maps of the predicted VWC (Figure 5) are compared to Figure 4a, it is clear that the regression calibrations preserve more of the detail in the spatial patterns compared to the z-score calibration predictions. The spatial patterns in the data for the z-score calibration (Figure 5d–f) are similar for all sample sizes, yet the z-score calibration does a better job at capturing the full range of values in the data

(see Table 1—minimum and maximum values for predicted data compared to the observed field VWC values in the first row) than the regression calibrations. The acceptable range of RMSEs for regression and z-score calibration (5–6%) was determined based on the range of RMSE values obtained from the Eca and drone surveys collected on the same day as the VWC surveys for the West Stadium field for the best-performing variables.

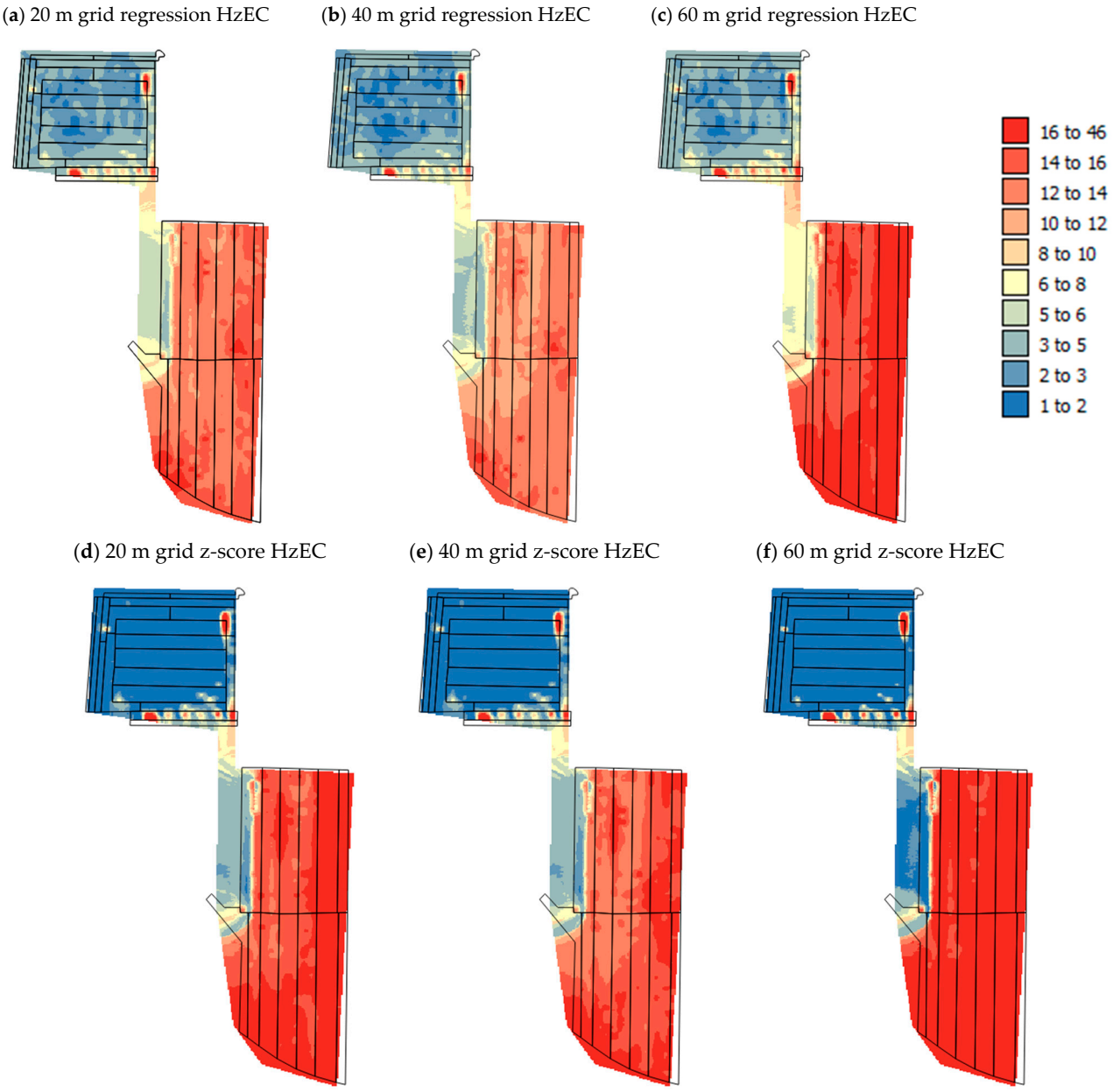

Figure 5. Kriged maps of the predicted VWCs for the West Stadium field on 24 May 2022 based on regression (**a**–**c**) and z-score calibration (**d**–**f**) using the HzEC data and different-sized sub-samples of data.

3.2. Harmon Field

3.2.1. Spatial Patterns in Variables

Figure 6 shows the VWC, HzEC, VtEC, Th.IR and RGB maps for the Harmon field. The various data were collected on slightly different dates. ECa data collected on 6 May, 9 May and 17 May were compared with VWC data from 4 May. The Th.IR and green reflectance data collected on 8 April were compared with VWC data from 26 April, and the Th.IR and RGB data for 12 October were compared with the VWC data from 6 October. Figure 6

shows the most similarity between the 4 May VWC (Figure 6a) and 6 May HzEC (r = 0.57), 9 May HzEC data (r = 0.53, Figure 6b) and 17 May HzEC data (r = 0.60, Figure 6e), but the patterns for the VtEC 9 May (r = 0.21, Figure 6c), VtEC 17 May (r = 0.27, Figure 6f), Th.IR 8 April (r = 0.03, Figure 5d), Th.IR 12 October (r = 0.11, Figure 6g) and RGB 12 October (r = 0.10, Figure 6h) are quite different. This difference in VtEC can be attributed to the deeper depth of inquiry than the HzEC and the VWC survey for topsoil (0–10 cm). For Th.IR, the difference likely relates, in part, to the longer time between the drone and VWC surveys but also differences in grass health being primarily captured in the drone imagery. Kerry et al. [37] showed that ground and drone surveys of NDVI and % dead grass present gave poorer indications of VWC spatial patterns than a human touching the grass and determining if it felt dry, damp or wet. This is because patterns in grass health observed by drone can be related to factors other than soil moisture, like the degree of trampling and compaction, lack of nutrients or management activities like mowing.

3.2.2. RMSEs for EC Data

As for the West Stadium field, the RMSEs for the Harmon field were generally lower for regression calibrations for all sample sizes (Table 2). The RMSEs were lowest for the z-score calibrations in a few cases (see bolded RMSEs in Table 2) or a very similar magnitude when just the sensor locations (just six locations) or the 45 m grid were used. Also, for a given date, the RMSEs were higher for the VtEC, as expected, given the different average inquiry depths for VtEC (1.5 m) and theta probes (0–10 cm) [68]. The RMSEs also show a general pattern of increasing for the HzEC and VtEC with increasing time between the VWC measurements being made in the field and the EC surveys, which is an expected pattern. The only exceptions to this pattern are the low RMSEs for HzEC 17 May and the low regression RMSEs for the 45 m grid for some of the later dates. This shows that patterns in soil moisture change with time and should probably be reassessed periodically. This finding is consistent with those of Liakos and Vellidis [44], O'Shaughnessy et al. [25] and Straw and Henry [48], yet it does not suggest that mapping should be redone before every irrigation event. This is in agreement with the findings of Straw et al. [49], who found that a single irrigation event did not markedly alter the spatial patterns of the VWC. If we take RMSEs with a magnitude around 5–6% as acceptable, as this was the magnitude of the lowest RMSEs for the West Stadium field where all data were collected on the same day, and if using sparse HzEC (45 m grid data) for the calibration, then the RMSEs were relatively stable for a period of about 3 weeks (Table 2). Also, the maps of the VWC for 4 May and HzEC for 9 May and 17 May (Figure 6a,b,e) have key features in common such as low values at the north end of the field and southwest corner as well as similar shapes in the large values in the center and southeast of the field.

In addition to the patterns of RMSEs in Table 2, the patterns in the minimum, maximum and mean values of the VWC predicted by both calibration methods and the EC data on different dates are important. There was a decrease in the range of regression-predicted VWC values with increased time between the field observations and the EC measurements. The minimum values got larger and the maximum values got smaller, as a result, while the mean predicted VWC stayed somewhat constant. The RMSEs appear similar, but the minimum and maximum values and the standard deviation are not modelled appropriately. For the z-score calibration, the range of values is greater than for the field observations, with the minimum value being lower (negative values) and the maximum value being higher than the field observations for the HzEC 6 May, 17 May and 30 May, as well as the VtEC 13 May and 23 May. However, the standard deviations are around 8% for most EC measurement dates and grid densities. This suggests that the z-score calibration approach better preserves a greater range of variability when calibrated with minimal data. This is also shown by the RMSE for the sensors (just six points) being very similar for the regression and z-score approaches (Table 2) while the minimum and maximum values from the z-score approach are much closer to the minimum and maximum values from the field observation data. This is similar to the findings of Kerry et al. [65] for several agricultural fields in the UK.

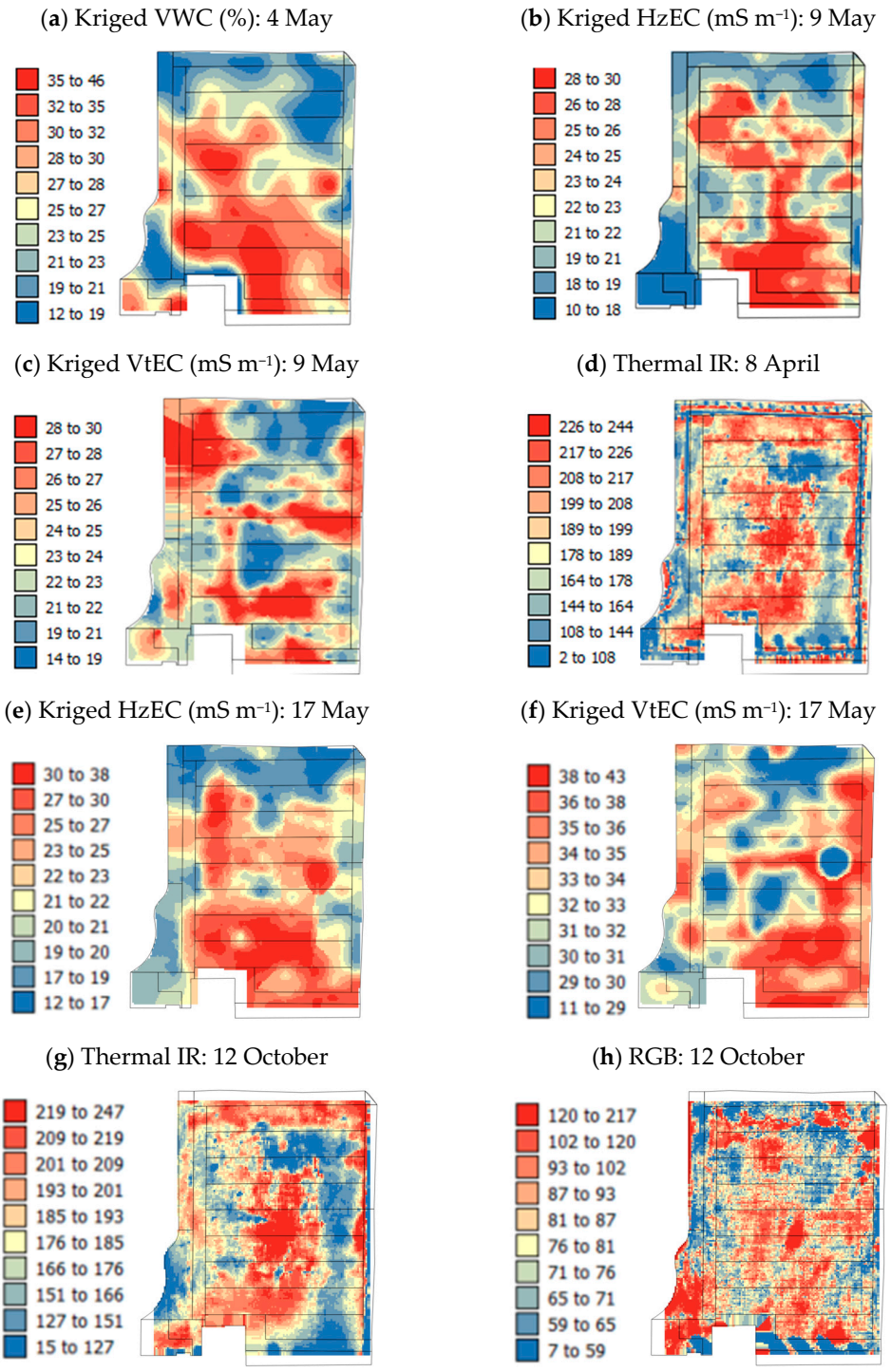

Figure 6. Kriged maps of the Harmon field in 2022 for the (**a**) VWC 4 May, (**b**) HzEC 9 May, (**c**) VtEC 9 May, (**d**) thermal IR 8 April, (**e**) HzEC 17 May, (**f**) VtEC 17 May, (**g**) thermal IR 12 October and (**h**) RGB 12 October.

The effect of the z-score calibration approach preserving the range in values better than the regression calibration approach is illustrated in Figure 7, where all predictions are plotted to the same scale as the field-observed VWC from 4 May (Figure 6a). All maps in Figure 7 have predictions that were produced using the HzEC data from 9 May. The range of values was well preserved for the 15 m, 30 m and 45 m data using the z-score approach, but for the regression approach, the range of values in the maps was only well reproduced by the 30 m and 45 m data. It is also clear that when only the six sensor locations

were used for calibration, the z-score calibration preserved the patterns of variation and ranges of values better than the regression calibration. This finding is similar to that of Kerry et al. [65], that when a very small sample size is used, transforming z-scores of sensed data to the scale of the soil variable (here VWC) performs better than using management zone averages. For the regression approach, it was hard to capture the full range of values with a small sample size, but the z-score calibration considered the standard deviation of the data, which helped preserve the full range of values.

Table 2. Summary statistics and RMSEs for the VWC predicted using ECa data calibrated using regression and z-scores for the Harmon field on various dates.

	Regression Calibration					z-Score Calibration				
Data	**Min.**	**Max.**	**Mean**	**St. Dev.**	**RMSE**	**RMSE**	**Min.**	**Max.**	**Mean**	**St. Dev.**
VWC 4 May 2022	12.83	45.64	26.74	6.22	–	–	12.83	45.64	26.74	6.22
HzEC 6 May 15 m	8.68	40.30	26.03	3.82	**5.15**	7.22	−13.24	57.68	25.67	8.56
HzEC 6 May 30 m	4.89	42.39	25.46	4.52	**5.34**	7.00	−11.76	56.16	25.51	8.20
HzEC 6 May 45 m	12.12	38.83	26.77	3.22	**5.11**	7.05	−12.05	57.31	26.01	8.37
HzEC 6 May sensors	22.01	31.55	27.24	1.15	5.66	**5.24**	16.24	36.22	27.02	2.41
HzEC 9 May 15 m	16.20	33.78	25.88	2.87	**5.36**	7.54	−3.18	49.22	25.67	8.56
HzEC 9 May 30 m	8.72	40.42	26.17	5.18	**5.64**	7.32	−2.12	48.07	25.51	8.20
HzEC 9 May 45 m	11.16	40.62	27.38	4.81	**5.53**	7.37	−2.21	49.05	26.01	8.37
HzEC 9 May sensors	13.81	37.28	26.73	3.83	**5.31**	5.37	19.07	33.84	27.02	2.41
VtEC 9 May 15 m	21.46	27.99	25.69	1.18	**6.23**	9.83	−5.07	42.46	25.67	8.56
VtEC 9 May 30 m	15.56	31.02	25.56	2.78	**6.52**	9.57	−3.94	41.59	25.51	8.20
VtEC 9 May 45 m	17.83	29.90	25.64	2.17	**6.36**	9.66	−4.06	42.43	26.01	8.37
VtEC 9 May sensors	24.59	28.40	27.06	0.69	**6.16**	6.33	18.54	31.93	27.02	2.41
HzEC 13 May 15 m	24.70	26.30	25.67	0.53	**7.00**	10.37	9.90	35.79	25.67	8.56
HzEC 13 May 30 m	23.15	26.91	25.44	1.24	**5.59**	10.10	10.20	35.19	25.51	8.19
HzEC 13 May 45 m	20.98	30.04	26.50	2.99	**3.77**	10.19	10.59	35.90	26.01	8.37
VtEC 13 May 15 m	20.46	36.59	25.84	1.74	**8.45**	9.39	−0.85	78.66	25.67	8.56
VtEC 13 May 30 m	17.11	42.39	25.54	2.72	**8.39**	9.13	0.14	76.21	25.51	8.19
VtEC 13 May 45 m	16.74	42.32	25.27	2.75	**8.13**	9.21	0.08	77.82	26.01	8.37
HzEC 17 May 15 m	18.16	36.48	26.03	3.21	**4.04**	7.01	4.73	53.50	25.67	8.56
HzEC 17 May 30 m	13.51	42.05	25.76	5.01	**1.44**	6.79	5.47	52.14	25.51	8.19
HzEC 17 May 45 m	14.84	42.31	26.64	4.82	**2.56**	6.84	5.53	53.23	26.01	8.37
VtEC 17 May 15 m	11.12	31.85	25.65	2.25	**8.96**	9.18	−29.58	49.26	25.67	8.56
VtEC 17 May 30 m	5.60	32.29	24.30	2.90	**7.95**	8.92	−27.36	48.08	25.51	8.19
VtEC 17 May 45 m	−2.80	38.67	26.26	4.50	10.71	**9.00**	−28.02	49.07	26.01	8.37
HzEC 23 May 15 m	24.70	26.30	25.67	0.53	**7.00**	10.37	9.90	35.79	25.67	8.56
HzEC 23 May 30 m	23.14	26.90	25.43	1.24	**5.58**	10.10	10.42	35.19	25.51	8.19
HzEC 23 May 45 m	20.98	30.04	26.50	2.99	**3.77**	10.19	10.59	35.90	26.01	8.37
VtEC 23 May 15 m	23.67	27.71	25.68	0.67	**7.97**	9.95	−0.07	51.75	25.67	8.56
VtEC 23 May 30 m	16.91	34.12	25.46	2.84	**8.08**	9.68	0.88	50.46	25.51	8.19
VtEC 23 May 45 m	24.88	27.12	26.01	0.37	**8.14**	9.77	0.84	51.51	26.01	8.37
VtEC 27 May 15 m	22.84	29.29	25.83	1.41	**6.25**	9.14	7.51	46.61	25.67	8.56
VtEC 27 May 30 m	19.10	34.05	26.04	3.27	**4.13**	8.88	8.14	45.55	25.51	8.19
VtEC 27 May 45 m	17.54	36.90	26.53	4.24	**3.41**	8.96	8.26	46.49	26.01	8.37
HzEC 30 May 15 m	18.38	34.84	25.67	2.65	**7.54**	7.90	2.07	55.34	25.67	8.56
HzEC 30 May 30 m	11.57	43.47	25.71	5.13	**7.28**	7.67	2.93	53.89	25.51	8.19
HzEC 30 May 45 m	22.80	30.26	26.11	1.20	8.15	**7.73**	2.93	55.02	26.01	8.37
VtEC 30 May 15 m	16.69	29.36	25.65	1.50	**7.76**	9.19	−25.52	46.93	25.67	8.56
VtEC 30 May 30 m	2.60	34.31	25.01	3.75	**7.00**	8.94	−23.46	45.85	25.51	8.19
VtEC 30 May 45 m	11.76	31.94	26.02	2.39	**8.08**	9.02	−24.04	46.79	26.01	8.37

Key: HzEC = electrical conductivity horizontal mode, VtEC = electrical conductivity vertical mode. **Bold** values show the lowest RMSEs for a given variable, sample size and date.

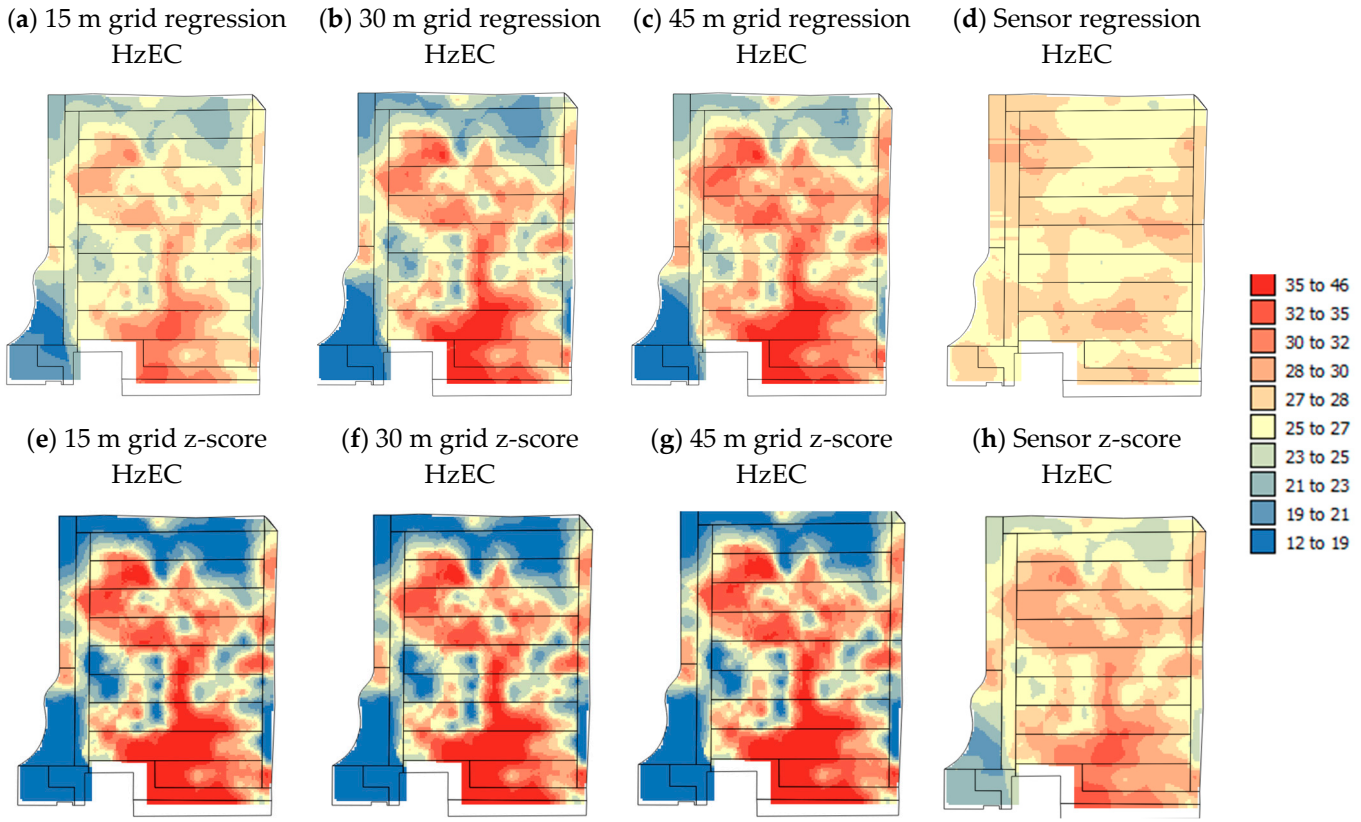

Figure 7. Maps of the VWC predictions produced using the HzEC and regression (**a**–**d**) and z-score calibration (**e**–**h**) for the Harmon field in 2022 for 9 May.

3.2.3. RMSEs for Drone Data

The regression RMSEs for drone Th.IR and the green waveband (Table 3) were of a similar magnitude to those for the EC, but those for Th.IR were generally larger (compare with Table 2). The April drone imagery was captured 18 days before the soil survey, so RMSEs might have been expected to be larger; however, the imagery and soil survey data were both collected before the irrigation season started. This might suggest that the patterns in soil moisture and reflectance and Th.IR are more indicative of the natural patterns of variation in this field without management effects, but patterns of greenness in April also reflect the timing of green-up after winter dormancy. In contrast, the first half of October 2022 had very hot weather and the sprinklers were still being used when the imagery and soil data were collected and were likely to have shown the full effects of the summer irrigation period. Nevertheless, the RMSEs were 2–3% higher on average than those for the April flight. Another interesting feature is that the RMSEs were higher for Th.IR in April, but lower for Th.IR in October.

For the z-score calibrations, the RMSEs are generally larger than those for the regression calibration, apart from for the sensor locations in April. For both types of calibration, the maximum values were frequently overestimated, but this was more the case for the z-score calibration, especially for the October flight. For the minimum values however, the regression calibration tended to markedly overestimate the minimum values and the z-score calibration underestimate them. These results suggest that using EC data to indicate patterns of spatial variation in soil moisture is more appropriate than using imagery data. This accords with the findings of Kerry and Oliver [73], who found that EC or bare soil aerial imagery was more strongly related to patterns in soil properties than imagery where there was a crop in the field. The turfgrass in this situation can be seen as having been responding to variations in more properties than just soil moisture and may have also been responding to differences in nutrients, trampling or compaction, mowing frequency

and direction, and pests like weeds. The turfgrass in April was also coming out of the winter senescent period and was not fully greened up, so it was not particularly reflecting differences in soil moisture. This finding accords with that of Kerry et al. [37], who showed that NDVI measurements made in the field gave the poorest indication of variation in the VWC of several variables that were investigated. They also showed that there were situations where there was a negative correlation between the NDVI and VWC due to damage to the turfgrass in wetter areas by mowers or sporting activities.

Table 3. Summary statistics and RMSEs for VWCs predicted using drone data calibrated using regression and z-scores for the Harmon field on various dates.

	Regression Calibration					z-Score Calibration				
Data	**Min.**	**Max.**	**Mean**	**St. Dev.**	**RMSE**	**RMSE**	**Min.**	**Max.**	**Mean**	**St. Dev.**
VWC 26 April 2022	−0.83	32.63	13.71	5.52	–	–	−0.83	32.63	13.71	5.52
Th.IR 8 April 15 m	19.75	28.15	25.76	1.63	**6.36**	10.18	−5.91	38.18	25.67	8.56
Th.IR 8 April 30 m	−4.29	40.74	27.97	8.74	10.34	**9.91**	−4.74	37.49	25.51	8.20
Th.IR 8 April 45 m	19.32	29.15	26.36	1.91	**6.35**	10.00	−4.88	38.25	26.02	8.37
Th.IR 8 April sensors	25.39	33.62	27.72	1.60	6.63	**6.48**	18.30	30.72	27.20	2.41
Gr. 8 April 15 m	20.00	33.52	25.83	1.82	**5.98**	8.95	−1.74	61.79	25.67	8.56
Gr. 8 April 30 m	18.07	36.63	26.08	2.50	**5.97**	8.70	−0.74	60.10	25.51	8.20
Gr. 8 April 45 m	20.48	34.02	26.32	1.82	**5.93**	8.78	−0.80	61.34	26.02	8.37
Gr. 8 April sensors	25.75	29.03	27.17	0.44	6.11	**5.95**	19.48	37.38	27.20	2.41
VWC 6 October 2022	14.07	43.22	29.74	7.52	–	–	14.07	43.22	29.74	7.52
RGB 5 October 15 m	20.50	35.18	29.11	2.44	**8.58**	15.75	−18.40	63.46	29.64	13.62
RGB 5 October 30 m	26.79	29.15	28.18	0.39	**8.41**	14.34	−13.47	57.79	28.35	11.86
RGB 5 October 45 m	19.18	27.16	23.86	1.33	**10.17**	16.54	−23.57	60.03	25.49	13.91
RGB 12 October 15 m	3.26	45.25	29.54	5.48	**9.43**	15.18	−35.73	68.70	29.64	13.62
RGB 12 October 30 m	11.48	38.11	28.15	3.47	**8.76**	13.79	−28.56	62.35	28.35	11.86
RGB 12 October 45 m	17.33	30.68	25.69	1.74	**9.19**	15.98	−41.27	65.38	25.49	13.91
Th.IR 12 October 15m	24.89	39.39	29.25	2.26	**8.35**	15.15	3.34	90.89	29.64	13.62
Th. IR 12 October 30m	23.25	37.10	27.41	2.15	**8.62**	13.76	5.45	81.66	28.35	11.86
Th.IR 12 October 45 m	21.28	33.01	24.80	1.83	**9.60**	15.95	−1.37	88.04	25.49	13.91

Key: Th.IR = thermal Infra-red, Gr. = Green, RGB = Red, Green, Blue. **Bold** values show the lowest RMSEs for a given variable, sample size and date.

In contrast to the April imagery, the October imagery may reflect the effects on the turfgrass health of water deficits earlier in the irrigation season. A solution to these issues might be to collect drone imagery early or towards the middle of the irrigation season; however, this was performed for the West Stadium site and the EC and drone imagery was collected on the same day as the soil survey. The HzEC still had lower RMSEs than the predictions from the drone imagery which suggests that the HzEC was the best variable for detecting variations in soil moisture in both the West Stadium and Harmon fields.

3.3. MTC Field

3.3.1. Spatial Patterns in Variables

Figure 8 shows the VWC for the MTC field on 5 May to compare with patterns in the HzEC and VtEC throughout the month of May. The VWC for 7 April can also be compared with the drone Th.IR and the green waveband maps from 8 April. In Figure 8, there is the most similarity between the 5 May VWC data and the 17 May VtEC data (r = 0.61), but the patterns for HzEC 17 May, HzEC 23 May and VtEC 27 May all have a common feature of an area of high values in the center of the field. However, the correlation coefficients with the 5 May VWC data are less than those for the 17 May VtEC (r = 0.44, r = 0.52 and r = 0.31, respectively). For Th.IR, there is a patch of low values in the center of the field and for the green waveband, a less well-defined area of high values in the center of the field. The correlations with 7 April VWC are low (r = −0.16 and r = 0.022, respectively). The greatest

similarity being between the 5 May VWC and the 17 May VtEC is unexpected given the difference in the depths of inquiry [68]. However, as mentioned in Section 2, a survey of soil texture along two transects in this field revealed some marked and unexpected changes in soil texture with depth, which may have influenced the topsoil VWC in places. What is apparent in the MTC field maps is the common feature that persists through time of an area of high VWC and ECa values and low Th.IR values in the center of the field. This coincides with an area close to an equipment shed where sporting activities were concentrated and which may have become compacted over time.

(**a**) Kriged VWC (%): 5 May

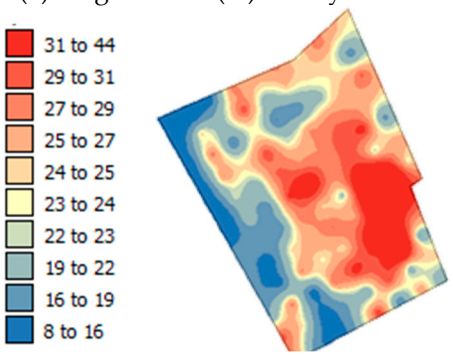

(**b**) Kriged HzEC (mS m^{-1}): 17 May

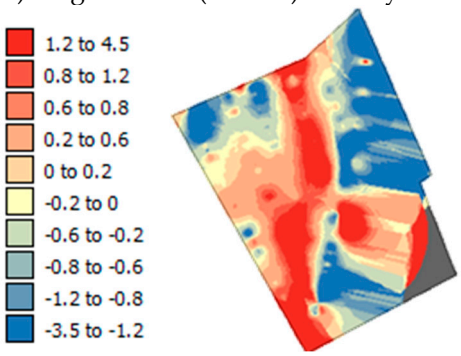

(**c**) Kriged VtEC (mS m^{-1}): 17 May

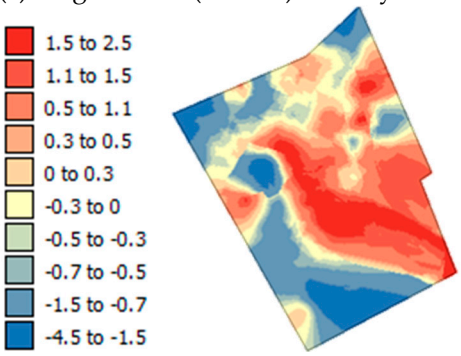

(**d**) Kriged HzEC (mS m^{-1}): 23 May

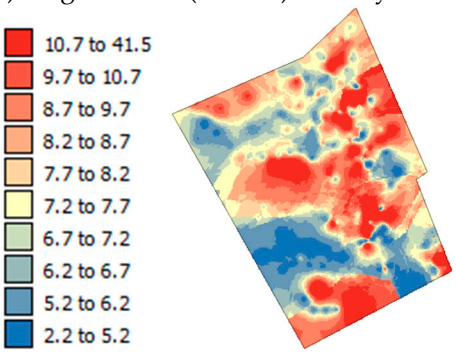

(**e**) Kriged VtEC (mS m^{-1}) 27 May

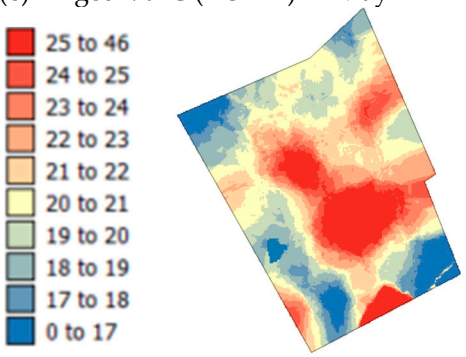

(**f**) Kriged VWC (%): 7 April

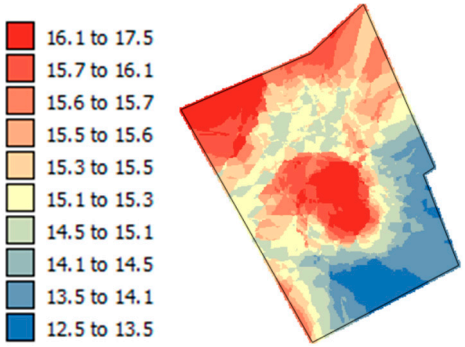

Figure 8. *Cont.*

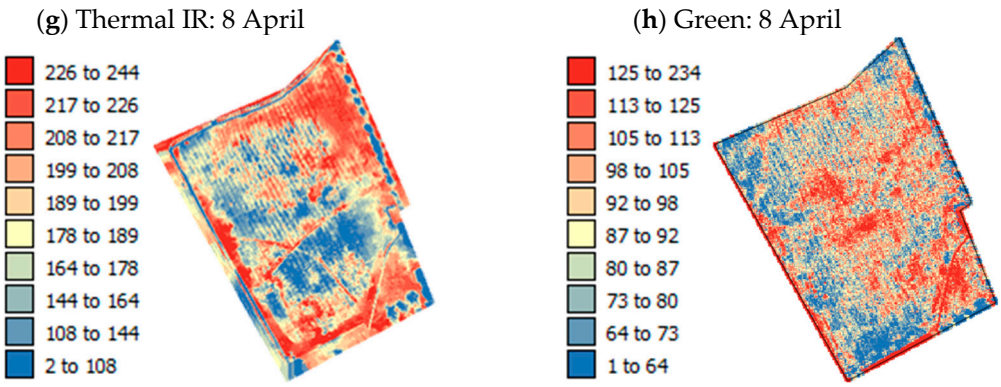

Figure 8. Kriged maps of the MTC field in 2022 for (**a**) VWC 5 May, (**b**) HzEC 17 May, (**c**) VtEC 17 May (**d**) HzEC 23 May, (**e**) VtEC 27 May, (**f**) VWC 7 April, (**g**) thermal IR 8 April and (**h**) green waveband 8 April.

3.3.2. RMSEs for EC Data

The RMSEs for the EC measurements on different dates in the MTC field compared to the 5 May VWC data are shown in Table 4. They are generally noticeably lower for the regression calibrations for all sample sizes, but the RMSEs for z-score calibrations using just the sensor locations were of a similar magnitude to the regression calibration RMSEs and were lower than the regression calibration RMSEs for about half of the dates investigated. The VtEC data had lower RMSEs than the HzEC data for 17 May, but this was not a consistent pattern for other dates, with the VtEC generally having similar, but slightly higher RMSEs for a given date than the HzEC. These same patterns were evident in the z-score RMSEs, but the RMSEs were generally larger. The lack of marked contrast in the RMSEs between the HzEC and VtEC was unexpected given the shallower relative depth of inquiry for HzEC [68] and the theta probes used for the topsoil VWC survey. However, although the Web Soil Survey (https://websoilsurvey.sc.egov.usda.gov/App/HomePage.htm, accessed on 1 March 2021) classifies the whole field as having sandy/gravelly loam texture, some big differences in soil texture within the field and with depth were observed as the field was developed on an alluvial fan. These textural differences could be the reason for the similar behavior of the HzEC and VtEC in this field. While there were greater RMSEs for 13 May than 9 May as might be expected with a larger interval of time between the VWC and EC surveys, there was not a consistent increase in RMSEs with increasing time between the VWC and EC surveys (Table 4). The RMSEs were smallest for the 17 May survey.

For the regression calibration (Table 4), the mean values were all quite close to the mean VWC measured on 5 May in the field, but the minimum and maximum values were consistently over- and underestimated, respectively. For the z-score calibration, the mean values are close to the mean for the 5 May VWC measurements. However, while there are some extremely low values for the minimum on particular dates for the z-score calibration, the maximum values are closer to the those for the 5 May VWC field survey than the maximum values for the regression calibration. Figure 9 shows maps of the predicted VWC from the regression and z-score calibrations and the various sub-samples using the 9 May HzEC data. They are all plotted to the same scale as the 5 May VWC values from the field survey (Figure 8a). It is clear from the patterns in the maps that the regression calibration produced maps with many values around the average VWC (Figure 9a–d), but the minimum and maximum values were preserved better for the z-score calibration and the patterns for the z-score calibration maps (Figure 8e–h) were more similar to those for the 5 May VWC survey (Figure 8a).

Table 4. Summary statistics and RMSEs for the VWCs predicted using ECa data calibrated using regression and z-scores for the MTC field on various dates.

	Regression Calibration					z-Score Calibration				
Data	**Min.**	**Max.**	**Mean**	**St. Dev.**	**RMSE**	**RMSE**	**Min.**	**Max.**	**Mean**	**St. Dev.**
VWC 5 May 2022	8.46	47.38	24.37	5.75	–	–	8.46	47.38	24.37	5.74
HzEC 9 May 20 m	16.08	35.63	24.08	3.66	**5.01**	5.05	7.44	47.69	23.92	7.53
HzEC 9 May 40 m	18.32	32.57	24.15	2.67	**4.96**	8.03	3.72	53.11	23.95	9.24
HzEC 9 May 60 m	17.29	30.05	22.52	2.39	**5.31**	7.12	5.81	47.88	23.04	7.87
HzEC 9 May sensors	19.80	33.01	25.21	4.65	**5.04**	5.05	17.97	35.89	25.31	3.35
VtEC 9 May 20 m	−58.32	27.26	23.94	1.49	**5.66**	8.53	−392.47	40.745	23.92	7.53
VtEC 9 May 40 m	−51.84	26.91	23.85	1.37	**5.66**	9.87	−487.00	44.59	23.95	9.24
VtEC 9 May 60 m	−152.80	29.38	22.31	3.17	**6.33**	8.88	−412.15	40.62	23.04	7.87
VtEC 9 May sensors	14.26	215.36	22.07	3.50	7.65	**6.12**	−160.10	32.80	25.31	3.35
HzEC 13 May 20 m	22.77	30.42	23.94	0.52	**5.74**	9.05	6.98	117.91	23.92	7.53
HzEC 13 May 40 m	23.43	26.96	23.97	0.24	**5.75**	10.43	3.17	139.26	23.95	9.24
HzEC 13 May 60 m	19.72	40.27	22.86	1.40	**5.98**	9.40	5.33	121.27	23.04	7.87
HzEC 13 May sensors	18.05	62.33	24.81	3.01	**6.25**	6.45	17.77	67.14	25.31	3.35
HzEC 17 May 20 m	23.64	24.28	24.02	0.10	**5.66**	9.41	4.47	51.65	23.92	7.53
HzEC 17 May 40 m	18.84	30.53	23.66	1.87	**5.60**	10.78	0.09	57.97	23.95	9.09
HzEC 17 May 60 m	17.03	31.07	22.82	2.24	**5.20**	9.75	2.70	52.01	23.04	7.45
HzEC 17 May sensors	17.76	29.14	24.45	1.82	**6.54**	6.70	16.65	37.65	25.31	3.30
VtEC 17 May 20 m	9.38	32.91	24.16	4.06	**4.52**	5.99	−3.53	40.19	23.92	7.53
VtEC 17 May 40 m	5.60	36.08	24.74	5.25	**4.80**	7.23	−9.72	43.91	23.95	9.24
VtEC 17 May 60 m	6.29	32.88	22.98	4.58	**4.80**	6.35	−5.65	40.04	23.04	7.87
VtEC 17 May sensors	20.35	29.09	25.84	1.51	5.16	**4.59**	13.09	32.55	25.31	3.35
HzEC 23 May 20 m	9.26	32.80	24.26	3.15	**4.90**	6.67	−11.95	44.33	23.92	7.53
HzEC 23 May 40 m	7.80	34.58	24.86	3.58	**4.95**	7.93	−20.06	49.00	23.95	9.24
HzEC 23 May 60 m	8.04	33.49	24.26	3.41	**4.91**	7.02	−14.45	44.38	23.04	7.87
HzEC 23 May sensors	12.77	47.54	25.38	4.65	9.15	**4.99**	9.34	34.40	25.31	3.35
VtEC 23 May 20 m	15.77	25.09	23.89	0.46	**5.77**	9.29	−107.89	43.53	23.92	7.53
VtEC 23 May 40 m	20.45	49.69	24.24	1.45	**5.99**	10.68	−137.79	48.02	23.95	9.24
VtEC 23 May 60 m	20.28	43.84	23.33	1.17	**6.01**	9.64	−114.72	43.54	23.04	7.87
VtEC 23 May sensors	9.44	130.10	25.07	6.00	8.51	**6.60**	−33.84	34.04	25.31	3.35
HzEC 27 May 20 m	15.54	33.29	24.08	2.55	**5.48**	7.85	−1.25	51.08	23.92	7.53
HzEC 27 May 40 m	17.86	31.08	24.22	1.90	**5.44**	9.16	−6.94	57.28	23.95	9.24
HzEC 27 May 60 m	13.28	33.62	23.06	2.93	**5.69**	8.20	−3.27	51.43	23.04	7.87
HzEC 27 May sensors	18.27	30.00	24.36	1.69	6.50	**5.71**	−16.33	25.68	25.31	3.35
VtEC 27 May 20 m	8.00	29.44	24.02	1.10	**5.51**	8.96	−69.58	24.76	23.92	7.53
VtEC 27 May 40 m	−3.76	33.21	23.87	1.90	**5.47**	10.33	90.79	24.98	23.95	9.24
VtEC 27 May 60 m	22.08	25.95	23.06	23.06	**5.96**	9.31	−74.68	23.91	23.04	7.87
VtEC 27 May sensors	−24.79	43.21	26.03	3.50	**5.94**	6.39	14.10	37.41	25.31	3.35
HzEC 30 May 20 m	19.31	29.37	24.07	1.84	**5.59**	8.28	4.41	45.63	23.92	7.53
HzEC 30 May 40 m	23.26	24.59	23.95	0.24	**5.83**	9.61	0.01	50.59	23.95	9.24
HzEC 30 May 60 m	16.91	28.73	23.14	2.16	**6.74**	8.63	2.65	45.73	23.04	7.87
HzEC 30 May sensors	18.02	34.38	25.77	2.99	**5.95**	5.97	16.62	34.98	25.31	3.35
VtEC 30 May 20 m	14.14	33.62	24.09	3.00	**5.42**	7.61	−1.04	47.80	23.92	7.53
VtEC 30 May 40 m	15.70	31.93	23.99	2.50	**5.37**	8.90	6.68	53.25	23.95	9.24
VtEC 30 May 60 m	12.06	33.50	23.02	3.31	**5.63**	7.95	3.05	47.99	23.04	7.87
VtEC 30 May sensors	11.49	41.72	26.94	4.66	6.44	**5.56**	14.20	35.94	25.31	3.35

Key: HzEC = electrical conductivity horizontal mode, VtEC = electrical conductivity vertical mode. **Bold** values show the lowest RMSEs for a given variable, sample size and date.

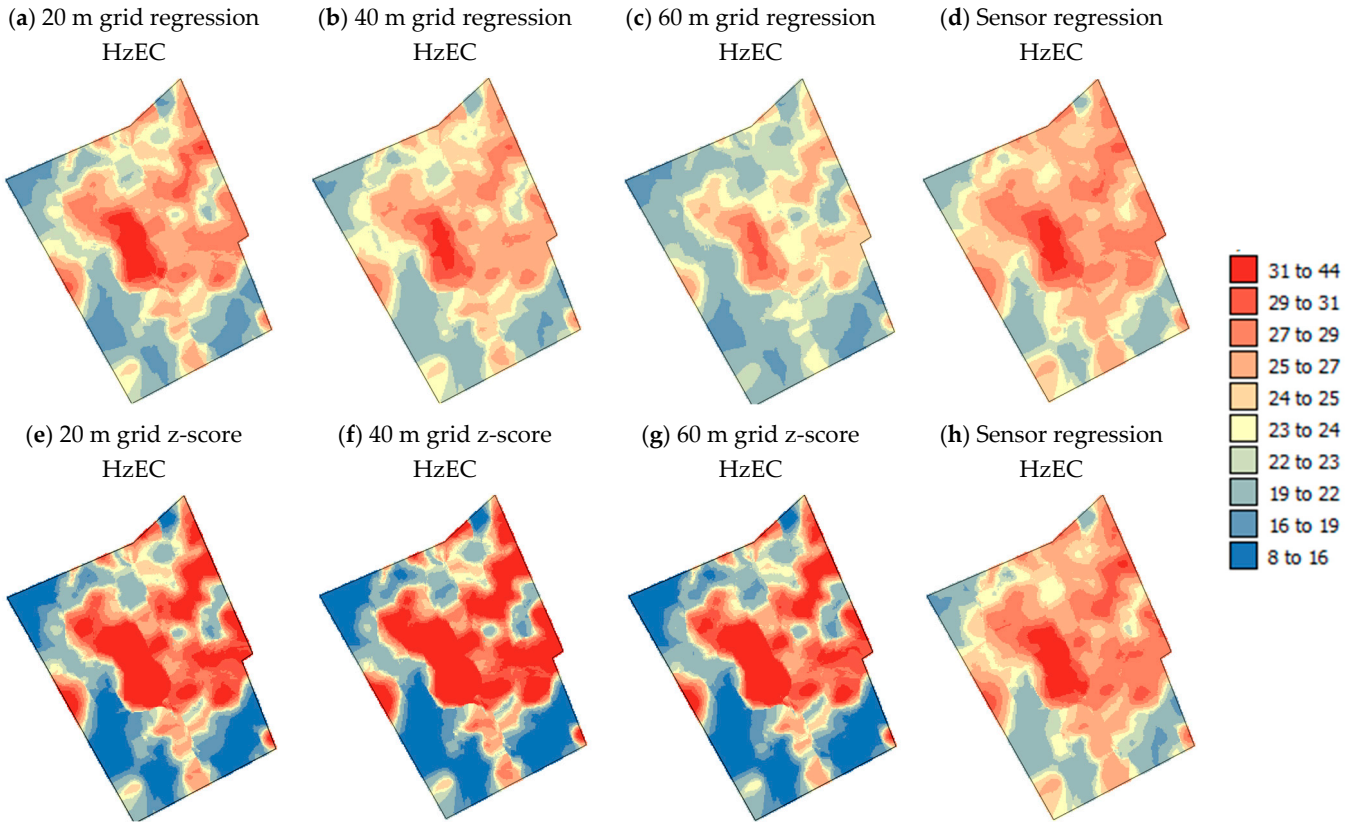

Figure 9. Maps of the VWC predictions produced using the HzEC and regression (**a**–**d**) and z-score calibration (**e**–**h**) for the MTC field in 2022 for 9 May.

3.3.3. RMSEs for Drone Data

The regression RMSEs for Th.IR and the green waveband for the 8 April imagery (Table 5) were far lower for the MTC field than the EC RMSEs, but those for the 19 May images (42 days later than the VWC survey in the field) were of a similar magnitude to the EC RMSEs (Table 4). This is probably due to there being just a day's difference in when the drone and soil surveys occurred. It is also probably a function of the far smaller range in VWC values on 7 April which were a result of a very dry winter and spring, but irrigation in the field had not yet commenced at the time of sampling. Also, the information for the other sites showed that the regression method better predicted to a narrow range of values. One of the October drone surveys was taken the same day as the VWC survey and only the RMSE for the 15 m data was less than 5. The drone data for 12 October had lower RMSEs than those for 5 October for both Gr. and Th.IR. This may be because due to scheduling and safety issues, to make sure the field was not full of people, the 5 October drone survey was undertaken at 4 pm whereas the 12 October survey was conducted at 12 noon when there were less shadows in the images and greater differences in Th.IR around the field. In addition to the time of day increasing shadow artefacts in images, it can impact soil moisture levels, with soil typically being drier in the afternoon compared to the early morning due to evaporation. These factors could influence covariates related to soil water content. Others have found that it is best to conduct drone surveys around noon to get the best lighting, minimize shadows and get similar illumination for all parts of the field [74]. This brings to light another drawback of frequent drone flights in an urban environment in heavily used fields.

Table 5. Summary statistics and RMSEs for the VWC predicted using drone data calibrated using regression and z-scores for the MTC field on various dates.

	Regression Calibration					z-Score Calibration				
Data	**Min.**	**Max.**	**Mean**	**St. Dev.**	**RMSE**	**RMSE**	**Min.**	**Max.**	**Mean**	**St. Dev.**
VWC 7 April 2022	11.93	16.19	14.40	0.93	–	–	11.93	16.19	14.40	0.93
Gr. 8 April 20 m	12.24	17.84	14.45	0.59	**1.09**	3.38	2.27	33.19	14.93	3.28
Gr. 8 April 40 m	13.84	15.22	14.77	14.38	**0.98**	3.19	3.20	32.19	14.66	14.66
Gr. 8 April 60 m	16.06	16.32	16.22	0.03	**2.04**	3.18	7.02	30.28	16.21	2.47
Gr. 8 April sensors	12.77	16.33	14.93	0.38	**1.14**	**1.14**	13.23	17.48	14.91	0.45
Th. IR 8 April 20 m	14.48	14.49	14.49	0.002	**0.93**	3.48	4.96	19.64	14.93	3.28
Th. IR 8 April 40 m	14.14	14.96	14.67	0.18	**1.00**	3.29	5.72	19.49	14.66	3.08
Th. IR 8 April 60 m	14.78	16.96	16.20	0.49	**2.10**	3.26	9.04	20.09	16.21	2.47
Th. IR 8 April sensors	14.83	14.93	14.93	0.02	**1.05**	1.18	13.60	15.62	14.91	0.45
Gr. 19 May 20 m	14.38	25.31	21.02	1.16	**6.98**	8.32	−3.84	66.99	23.92	7.53
Gr. 19 May 40 m	22.88	23.56	23.29	0.07	**5.87**	9.65	−10.11	76.81	23.95	9.24
Gr. 19 May 60 m	24.28	24.39	24.32	0.01	**5.75**	8.66	−5.98	68.06	23.04	7.87
Gr. 19 May sensors	28.54	28.55	28.55	0.001	7.11	**5.99**	12.94	44.49	25.31	25.31
Th. IR 19 May 20 m	21.24	25.62	25.08	0.63	**5.85**	9.35	17.57	69.47	23.92	7.53
Th. IR 19 May 40 m	22.81	22.88	22.89	0.01	**5.94**	10.74	16.15	79.83	26.95	9.24
Th. IR. 19 May 60 m	28.44	28.45	28.45	0.001	**7.05**	9.70	16.40	70.64	23.04	7.87
Th. IR. 19 May sensors	24.31	24.31	24.31	0.001	**5.75**	6.64	22.48	45.59	25.31	3.53
VWC 5 October 2022	21.97	41.99	34.81	4.03	–	–	21.97	41.99	34.81	4.03
Gr. 5 October 20 m	33.88	34.28	34.13	0.05	**4.08**	11.92	1.79	86.83	34.13	11.05
Gr. 5 October 40 m	25.59	25.64	25.63	0.01	**10.03**	10.08	6.94	75.68	33.08	8.93
Gr. 5 October 60 m	22.39	22.40	22.40	0.001	13.05	**11.57**	2.34	84.01	33.40	10.61
Gr. 12 October 20 m	32.15	37.60	34.11	0.82	**4.02**	11.05	7.83	80.87	34.13	11.05
Gr. 12 October 40 m	37.00	37.42	37.27	0.06	**4.73**	9.25	11.82	70.86	33.08	8.93
Gr. 12 October 60 m	27.91	27.95	27.93	0.006	**7.97**	14.15	8.14	78.28	33.40	10.61
Th. IR 12 October 20 m	20.48	39.23	34.50	4.33	**4.26**	9.77	−1.61	46.21	34.13	11.05
Th. IR 12 October 40 m	26.91	27.64	27.46	0.17	8.34	**8.00**	4.19	42.84	33.08	8.93
Th. IR 12 October 60 m	17.49	17.57	17.55	0.02	17.72	**14.64**	−0.92	44.99	33.40	10.61

Key: Th.IR = thermal Infra-red, Gr. = Green. **Bold** values show the lowest RMSEs for a given variable, sample size and date.

The RMSEs for the z-score calibration were generally larger than those for the regression calibration (Table 5), but they were sometimes lower for the sparsest data. The mean values for the VWC were well predicted by the regression and z-score approach for drone surveys that occurred within a week of the VWC survey, but the 19 May imagery markedly overestimated the mean VWC values. This shows that relatively recent drone data need to be used for mapping and zones may need to be reassessed periodically as Liakos and Vellidis [44], O'Shaughnessy et al. [25], and Straw and Henry [48] have suggested. Indeed, these results suggest that soil moisture patterns should be reassessed every few weeks at least. Also, as variable irrigation rates are applied to different zones, the management effect will end up changing spatial patterns in relation to initial patterns as Adamchuk et al. [63], Kerry et al. [66] and Kerry et al. [64] have shown. The accuracy of the 8 April drone data predictions is likely due to the fact that the minimum and maximum values were very close to the mean as there was so little variation in soil moisture in this pre-irrigation season, with very dry sampling time. For the VWC predictions based on regression calibration, minimum and maximum VWC predictions tended to be over- and underestimated, respectively, whereas for the z-score VWC predictions, the reverse patterns are evident in the minimum and maximum values.

4. Conclusions

Very little research has occurred into determining spatial zones for precision turfgrass irrigation. Drone and ECa data have been extensively used in precision agriculture for defining variable rate application zones, so this research endeavored to determine if they could be equally useful and economical in the context of precision turfgrass irrigation in providing dense sensed datasets that were related to soil moisture. This research showed that HzEC and drone data collected on the same date or within a week of soil survey data gave predictions with a similar degree of accuracy (RMSE ~ 5%). The findings from our study not only enhance the efficiency of water use in turfgrass management but also contribute to Sustainable Development Goals 6 (Clean Water and Sanitation) and 12 (Responsible Consumption and Production) by advocating for more targeted irrigation practices that reduce water waste, optimize resource use and minimize environmental impact [75].

HzEC generally gave more accurate predictions of topsoil VWC than VtEC, which is be expected given the greater similarity in the average depth of inquiry for the EM38 in the horizontal position and theta probe measurements. Nevertheless, at the MTC site, perhaps due to noticeable variations in soil texture that occurred with depth in the field, there was not a marked difference in the performance of the HzEC and VtEC when all the EC survey dates were considered. HzEC also generally gave slightly better predictions than drone data as the drone data were reflecting grass health as opposed to soil moisture, and grass health is affected by more things than just soil moisture, such as compaction or when mowing had last taken place. The best predictions from drone data occurred when there was very little variation in soil moisture pre-season, so these data were not a good indication of the general performance of the drone data.

The EC survey data from multiple dates, particularly for the Harmon field, showed that the greater the time between the EC and soil surveys, the greater the prediction errors were. This is not a surprising result. However, once the EC data were collected a few weeks after the VWC surveys, the RMSEs rose to ~8%. Although the RMSEs were generally lower for regression calibrations when there was just data from sensors or a very small sample size, the z-score calibration approach could be recommended. The use of the z-score calibration could also be recommended for its ability to predict the range of VWC values better as shown by the minimum and maximum predicted values and the maps comparing the predictions from the different approaches with the various sub-samples.

It is expected that the pattern of VWC would remain similar over time as it is largely related to topography and soil texture patterns, which are permanent properties of individual fields. However, turfgrass also uses different amounts of water spatially and this work shows the constant slight changes in the patterns of the VWC that need to be regularly monitored for effective precise irrigation management. Nevertheless, as shown in previous studies, it is unlikely that soil moisture zones would need to be reassessed before every irrigation event [49] and it is likely that field managers have significant knowledge of the variation in their fields which could be used in helping to define static irrigation zones [51]. This analysis shows that key features of patterns in the VWC and related variables are evident in maps that were produced two–three weeks apart. This could inform the relative frequency of sensing to inform temporally varying VRI zones for turfgrass or could be evidence that static zones could be used that were centered on these key features. In terms of practical applications, these findings advocate for the strategic placement of a minimal number of sensors in the areas of stable key features, which would reduce the need for dense, repetitive field surveys. This not only ensures cost efficiency but also supports long-term sustainability by adapting irrigation practices to the nuanced needs of the field, reducing unnecessary water and energy use.

For defining temporally varying irrigation zones, an EM38 instrument could be attached to lawn mowers and the filtering of highly conductive points and mapping could be automated relatively easily once identified. Some data would still be needed for calibration of the HzEC data before it was used for VWC mapping. Given the analysis presented here

and the cost of mapping increasing in line with the sample number, we suggest that a minimal number of sensors (5–10) could be installed in locations that coincided with the key features in the variation that seemed to be stable in time such as the large VWC values in the center of the MTC field, or that a field manager could use a theta probe to check the VWC in these key areas so that repeated dense field surveys would not be needed. A z-score calibration approach could be used for the automated mapping of soil moisture patterns as this was often more accurate with the sparser sample sizes (i.e., just at sensor locations) and preserved the range of the VWC values better than the regression approach.

4.1. Limitations

This study was subject to several limitations, particularly associated with the increased difficulty of collecting ECa and drone data in an urban environment.

Administrative approvals are needed for each drone flight on a university campus and there can be scheduling issues associated with busy sports fields. There are also more general restrictions on drone flights in urban areas than rural areas. For example, drone flights are forbidden over some urban fields due to their proximity to an airport or hospital helicopter pad. Also, drone images are affected by the time of day they are taken and management of the grass such as mowing and dead grass being left on the surface. Drone flights should be performed as close to noon as possible, but the October drone surveys of the MTC field highlighted the problems that resulted from scheduling issues for busy sports fields.

Measuring the ECa is also more complex in the urban environment. The EM38 picked up many conductive features in the urban context whose effects had to be removed before the spatial patterns in ECa could be assessed. Consequently, the sensing approaches used in this study were still relatively labor-intensive. It would probably be easiest to automate the collection of HzEC data, yet this would only be possible where there were sufficient funds to purchase an EM38 such as a golf course or high-income sports fields.

This study was limited by the timing of the field, ECa and drone surveys which were curtailed from being taken in the peak of irrigation season as sports camps were continuously held on these fields in June–August. This also shows that continual sensing (drone flights) that cannot be combined with routine field management activities like mowing (ECa surveys) are not likely to be practical or economic in the long run.

4.2. Future Work

Given that some key features in the variation were evident for a few weeks with intervening rain and irrigation events for both the Harmon and MTC fields, future work should explore the permanence of observed spatial variations. This could potentially guide the development of static irrigation zones that could further reduce operational costs and environmental impacts. This could lead to more refined policies and practices that not only benefit sports field management but also contribute to broader urban sustainability efforts, engaging stakeholders across various sectors to adopt and support these precision-based methods.

Author Contributions: Conceptualization, R.K., B.I., N.H. and B.H.; methodology, R.K., B.I., K.S., A.H., K.H., D.H., N.H. and R.J.; software, R.K., B.I. and K.H.; validation, R.K.; formal analysis, R.K., B.I., K.S., A.H., and K.H.; investigation, R.K.; resources, R.K., D.H., N.H., R.J. and B.H.; data curation, R.K.; writing—original draft preparation, R.K.; writing—review and editing, R.K., B.I., K.H. and B.H.; visualization, R.K., B.I., K.S., A.H. and K.H.; supervision, R.K., N.H., R.J. and B.H.; project administration, R.K., N.H., and B.H.; funding acquisition, R.K., N.H. and B.H. All authors have read and agreed to the published version of the manuscript.

Funding: This research was funded by The Charles Redd Center for Western Studies (https://reddcenter.byu.edu/, accessed on 1 May 2024).

Data Availability Statement: To access the data please contact the corresponding author.

Acknowledgments: The authors would like to thank the following additional students for their assistance with fieldwork: S. Harris, H. Kerry, A. Olson, S. Shumate and A. Welling.

Conflicts of Interest: The authors declare no conflicts of interest. The funders had no role in the design of the study; in the collection, analyses or interpretation of data; in the writing of the manuscript; or in the decision to publish the results.

References

1. Coats, S.; Smerdon, J.E.; Cook, B.I.; Seager, R. Are Simulated Megadroughts in the North American Southwest Forced? *J. Clim.* **2015**, *28*, 124–142. [CrossRef]
2. Harvey, C. Climate Change Has Helped Fuel a Megadrought in the Southwest. *E&E News*, 17 April 2020.
3. Williams, A.P.; Cook, E.R.; Smerdon, J.E.; Cook, B.I.; Abatzoglou, J.T.; Bolles, K.; Baek, S.H.; Badger, A.M.; Livne, B. Large contribution from anthropogenic warming to an emerging North American megadrought. *Science* **2020**, *368*, 314–318. [CrossRef]
4. Abbott, B.W.; Baxter, B.K.; Busche, K.; de Freitas, L.; Frei, R.; Gomez, T.; Karren, M.A.; Buck, R.L.; Price, J.; Frutos, S.; et al. Emergency Measures Needed to Rescue Great Salt Lake from Ongoing Collapse. 2023. Available online: https://pws.byu.edu/GSL%20report%202023 (accessed on 30 May 2024).
5. Derouin, S. Utah's Great Salt Lake has Lost Half of its Water Due to Thirsty Humans. *Science* **2017**. [CrossRef]
6. Wine, M.L.; Laronne, J.B. In Water-Limited Landscapes, an Anthropocene Exchange: Trading Lakes for Irrigated Agriculture. *Earth's Future* **2020**, *8*, e2019EF001274. [CrossRef]
7. Kem, C. Gardner Policy Institute. Census 2020: Utah Fastest Growing State in the US. 2021. Available online: https://gardner.utah.edu/news/utah-population-reaches-estimated-3343552-people-net-in-migration-surges/#:~:text=Gardner%20Policy%20Institute,%20indicate%20the,is%20the%20highest%20since%202017 (accessed on 13 March 2024).
8. Banta, M.; Utah Cities Added Hundreds of Thousands of People in a Decade. Salt Lake Tribune. 4 August 2023. Available online: https://www.sltrib.com/news/2023/08/04/most-utahs-growth-happens-1-its/ (accessed on 13 April 2024).
9. Milesi, C.; Running, S.W.; Elvidge, C.D.; Dietz, J.B.; Tuttle, B.T.; Nemani, R.R. Mapping and Modeling the Biogeochemical Cycling of Turf Grasses in the United States. *Environ. Manag.* **2005**, *36*, 426–438. [CrossRef]
10. Fidanza, M.; Turfgrass Is Not the Largest Irrigated Crop. June 2022. Available online: https://gcmonline.com/course/environment/news/turfgrass-crop-irrigation (accessed on 30 May 2024).
11. AghaKouchak, S.; Sorooshian, S.; Hsu, K.; Gao, X. The Potential of Precipitation Remote Sensing for Water Resources Vulnerability Assessment in Arid Southwestern United States. In *Climate Vulnerability*; Pielke, R.A., Ed.; Academic Press: San Diego, CA, USA, 2013; pp. 141–149.
12. EPA. Water Efficiency Management Guide: Landscaping and Irrigation. 832-F-17-016b. Environmental Protection Agency. 2017. Available online: https://www.epa.gov/sites/default/files/2017-12/documents/ws-commercialbuildings-waterscore-irrigation-landscape-guide.pdf (accessed on 11 April 2024).
13. Fisher, M.J.; Rao, I.M.; Ayarza, M.A.; Lascano, C.E.; Sanz, J.I.; Thomas, R.J.; Vera, R.R. Carbon Storage by Introduced Deep-Rooted Grasses in the South American Savannas. *Nature* **1994**, *371*, 236–238. [CrossRef]
14. Dass, P.; Houlton, B.Z.; Wang, Y.; Warlind, D. Grasslands May Be More Reliable Carbon Sinks Than Forests in California. *Environ. Res. Lett.* **2018**, *13*, 074027. [CrossRef]
15. Wood, R.A.; Burchett, M.D.; Alquezar, R.; Orwell, R.L.; Tarran, J.; Torpy, F. The Potted-Plant Microcosm Substantially Reduces Indoor Air VOC Pollution: I. Office Field-Study. *Water Air Soil Pollut.* **2006**, *175*, 163–180. [CrossRef]
16. Gibbons, P.; Gill, A.M.; Shore, N.; Moritz, M.A.; Dovers, S.; Cary, G.J. Options for Reducing House-Losses during Wildfires without Clearing Trees and Shrubs. *Landsc. Urban Plan.* **2018**, *174*, 10–17. [CrossRef]
17. Carrow, R.N.; Krum, J.M.; Flitcroft, I.; Cline, V. Precision Turfgrass Management: Challenges and Field Applications for Mapping Turfgrass Soil and Stress. *Precis. Agric.* **2010**, *11*, 115–134. [CrossRef]
18. Carrow, R.N.; Cline, V. Precision Turfgrass Management for Athletic Fields. SportsTurf, July 2011. Available online: https://sturf.lib.msu.edu/article/2011jul16.pdf (accessed on 30 May 2024).
19. Krum, J.M.; Carrow, R.N.; Karnok, K. Spatial Mapping of Complex Turfgrass Sites: Site-Specific Management Units and Protocols. *Crop Sci.* **2010**, *50*, 301–315. [CrossRef]
20. Fenton, J.P. *On-Farm Experience of Precision Agriculture*; The International Fertiliser Society: York, UK, 1998.
21. Earth Institute, Columbia University. 2010. Available online: https://blogs.ei.columbia.edu/2011/03/15/a-solution-to-the-problem-of-lawns/ (accessed on 30 May 2024).
22. Evans, S.R.; Kopp, K.; Johnson, P.G.; Hopkins, B.G.; Dai, X.; Schaible, C. Comparing Smart Irrigation Controllers for Turfgrass Landscapes. *HortTechnology* **2022**, *32*, 415–424. [CrossRef]
23. Serena, M.; Leinauer, B.; Velasco-Cruz, C.; Sevostianova, E. Optimizing frequency and amount of irrigation needed to establish cool-season turfgrasses. *Agron. J.* **2022**, *114*, 1851–1858. [CrossRef]
24. Serena, M.; Velasco-Cruz, C.; Friell, J.; Schiavon, M.; Sevostianova, E.; Sallenave, B.R.; Leinauer, B. Irrigation scheduling technologies reduce water use and maintain turfgrass quality. *Agron. J.* **2020**, *112*, 3456–3469. [CrossRef]
25. O'Shaughnessy, S.A.; Evett, S.R.; Colaizzi, P.D. Dynamic Prescription Maps for Site-Specific Variable Rate Irrigation of Cotton. *Agric. Water Manag.* **2015**, *159*, 123–138. [CrossRef]

26. Throssell, C.; Reicher, Z. Irrigation Practices for Homelawns. *Purdue Extension*. 2024. Available online: https://www.extension.purdue.edu/extmedia/ay/ay-7-w.pdf (accessed on 1 March 2024).
27. Sandor, D. Smart Irrigation Month. University of Minnesota. 2019. Available online: https://turf.umn.edu/news/smart-irrigation-month (accessed on 1 March 2024).
28. Bastug, R.; Buyuktas, D. The effects of different irrigation levels applied in golf courses on some quality characteristics of turfgrass. *Irrig. Sci.* **2003**, *22*, 87–93. [CrossRef]
29. Miller, G.L. Analysis of Soccer Field Surface Hardness. In Proceedings of the First International Conference on Turfgrass Management and Science for Sports Fields, Leuven, Belgium, 12–16 September 2004; Nektarios, P.A., Ed.; ISHS: Leuven, Belgium, 2004; pp. 287–294.
30. Caple, M.; James, I.; Bartlett, M. Spatial Analysis of the Mechanical Behaviour of Natural Turf Sports Pitches. *Sports Eng.* **2012**, *15*, 143–157. [CrossRef]
31. Freeland, R.S.; Sorochan, J.C.; Goddard, M.J.; McElroy, J.S. Using Ground-Penetrating Radar to Evaluate Soil Compaction of Athletic Turfgrass Fields. *Appl. Eng. Agric.* **2008**, *24*, 509–514. [CrossRef]
32. Flitcroft, I.; Krum, J.M.; Carrow, R.N.; Rice, K.; Carson, T.; Cline, V. Spatial Mapping of Penetrometer Resistance on Turfgrass Soils for Site-Specific Cultivation. In Proceedings of the 10th International Conference on Precision Agriculture, Denver, CO, USA, 18–21 July 2010; ISPA: Monticello, IL, USA, 2010.
33. Hong, M.; Bremer, D.J.; van der Merwe, D. Thermal Imaging Detects Early Drought Stress in Turfgrass Utilizing Small Unmanned Aircraft Systems. *Agrosyst. Geosci. Environ.* **2019**, *2*, 1–9. [CrossRef]
34. Hong, M.U.; Bremer, D.J.; van Der Merwe, D. Using Small Unmanned Aircraft Systems for Early Detection of Drought Stress in Turfgrass. *Crop Sci.* **2019**, *59*, 2829–2844. [CrossRef]
35. Viscarra-Rossel, R.A.; McBratney, A.B. Soil Chemical Analytical Accuracy and Costs: Implications from Precision Agriculture. *Aust. J. Exp. Agric.* **1998**, *38*, 765–775. [CrossRef]
36. Webster, R.; Oliver, M.A. Sample Adequately to Estimate Variograms of Soil Properties. *J. Soil Sci.* **1992**, *43*, 177–192. [CrossRef]
37. Kerry, R.; Ingram, B.; Hammond, K.; Shumate, S.; Gunther, D.; Jensen, R.R.; Schill, S.; Hansen, N.C.; Hopkins, B.G. Spatial Analysis of Soil Moisture and Turfgrass Health to Determine Zones for Spatially Variable Irrigation Management. *Agronomy* **2023**, *13*, 1267. [CrossRef]
38. Kerry, R.; Escolà, A. *Sensing Approaches for Precision Agriculture*; Springer Nature: Cham, Switzerland, 2021. [CrossRef]
39. Straw, C.M. Evaluation of Sampling Procedures for Spatial Analysis of Surface and Edaphic Properties on Sports Fields. Master's Thesis, University of Georgia, Athens, GA, USA, 2014.
40. Burbink, C.; Straw, C. Spatiotemporal variability of a stadium football pitch during a professional tournament. *Sports Eng.* **2023**, *26*, 8. [CrossRef]
41. Carlson, M.G.; Gaussoin, R.E.; Puntel, L.A. A review of precision management for golf course turfgrass. *Crop Forage Turfgrass Manag.* **2022**, *8*, e20183. [CrossRef]
42. Espevig, T.; Aamlid, T.S. Effects of root zone composition and irrigation regime on performance of velvet bentgrass putting greens. II. Thatch, root development and playability. *Acta Agricult. Scand. Sect. B Soil Plant Sci.* **2012**, *62* (Suppl. 1), 106–112. [CrossRef]
43. Straw, C.; Friell, J.; Horgan, B. Precision Irrigation for Golf Courses Using Sensor and Mapping Technologies. 2019. Available online: https://conservancy.umn.edu/handle/11299/214353 (accessed on 13 March 2024).
44. Liakos, V.; Vellidis, G. Sensing with Wireless Sensor Networks. In *Sensing Approaches for Precision Agriculture*; Kerry, R., Escolà, A., Eds.; Springer Nature: Cham, Switzerland, 2021; pp. 133–157.
45. Straw, C.; Bolton, C.; Young, J.; Hejl, R.; Friell, J.; Watkins, E. Soil Moisture Variability on Golf Course Fairways across the United States: An Opportunity for Water Conservation with Precision Irrigation. *Agrosyst. Geosci. Environ.* **2022**, *5*, e20323. [CrossRef]
46. Yue, C.; Lai, Y.; Watkins, E.; Patton, A.; Braun, R. A Behavioral Approach to Identify Barriers to Adoption of New Technology: A Case Study of Low-Input Turfgrasses. *J. Agric. Appl. Econ.* **2023**, *55*, 72–99. [CrossRef]
47. Swensen, A.; Kerry, R. Incentivized Efficient Watering Practices in Five Western States with a Focus on Utah. In Proceedings of the AAG Annual Meeting, Honolulu, HI, USA, 16–20 April 2024.
48. Straw, C.M.; Henry, G.M. Spatiotemporal Variation of Site-Specific Management Units on Natural Turfgrass Sports Fields during Dry Down. *Precis. Agric.* **2018**, *19*, 395–420. [CrossRef]
49. Straw, C.; Grubbs, R.A.; Henry, G.M. Short-Term Spatiotemporal Relationship between Plant and Soil Properties on Natural Turfgrass Sports Fields. *Agrosyst. Geosci. Environ.* **2020**, *3*, e20043. [CrossRef]
50. Straw, C.M.; Henry, G.M.; Shannon, J.; Thompson, J.J. Athletes' Perceptions of within-Field Variability on Natural Turfgrass Sports Fields. *Precis. Agric.* **2019**, *20*, 118–137. [CrossRef]
51. Straw, C.M.; Wardrop, W.S.; Horgan, B.P. Golf Course Superintendents' Knowledge of Variability within Fairways: A Tool for Precision Turfgrass Management. *Precis. Agric.* **2020**, *21*, 637–654. [CrossRef]
52. Adamchuk, V.I.; Hummel, J.W.; Morgan, M.T.; Upadhyaya, S.K. On-the-go soil sensors for precision agriculture. *Comput. Electron. Agric.* **2004**, *44*, 71–91. [CrossRef]
53. Brevik, E.C.; Fenton, T.E.; Lazari, A. Soil electrical conductivity as a function of soil water content and implications for soil mapping. *Precis. Agric.* **2006**, *7*, 393–404. [CrossRef]
54. Kühn, J.; Brenning, A.; Wehrhan, M.; Koszinski, S.; Sommer, M. Interpretation of Electrical Conductivity Patterns by Soil Properties and Geological Maps for Precision Agriculture. *Precis. Agric.* **2009**, *10*, 490–507. [CrossRef]

55. Adao, T.; Hruska, J.; Padua, L.; Bessa, J.; Peres, E.; Morais, R.; Sousa, J.J. Hyperspectral imaging: A review on UAV-based sensors, data processing and applications for agriculture and forestry. *Remote Sens.* **2018**, *9*, 1110. [CrossRef]
56. Agili, H.; Chokmani, K.; Cambouris, A.; Perron, I.; Poulin, J. Site-Specific Management Zones Delineation Using Drone-Based Hyperspectral Imagery. In Proceedings of the 14th International Conference for Precision Agriculture, Montreal, QC, Canada, 24–27 June 2018; Available online: https://ispag.org/proceedings (accessed on 1 May 2024).
57. Alchanatis, V.; Cohen, Y.; Cohen, S.; Moller, M.; Sprinstin, M.; Meron, M.; Tsipris, J.; Saranga, Y.; Sela, E. Evaluation of different approaches for estimating and mapping crop water status in cotton with thermal imaging. *Precis. Agric.* **2010**, *11*, 27–41. [CrossRef]
58. Cohen, Y.; Alchanatis, V.; Meron, M.; Saranga, Y.; Tsipris, J. Estimation of leaf water potential by thermal imagery and spatial analysis. *J. Exp. Bot.* **2005**, *56*, 1843–1852. [CrossRef]
59. Cohen, Y.; Alchanatis, V.; Sela, E.; Saranga, Y.; Cohen, S.; Meron, M.; Bosak, A.; Tsipris, J.; Ostrovsky, V.; Orolov, V.; et al. Crop water status estimation using thermography: Multi-year model development using ground-based thermal images. *Precis. Agric.* **2015**, *16*, 311–329. [CrossRef]
60. Cohen, Y.; Vellidis, G.; Campillo, C.; Liakos, V.; Graff, N.; Saranga, Y.; Snider, J.L.; Casadesús, J.; Millán, S.; del Henar Prieto, M. Applications of Sensing to Precision Irrigation. In *Sensing Approaches for Precision Agriculture*; Kerry, R., Escolà, A., Eds.; Springer: Cham, Switzerland, 2021; p. 415.
61. Straw, C.M.; Grubbs, R.A.; Tucker, K.A.; Henry, G.M. Handheld versus Mobile Data Acquisitions for Spatial Analysis of Natural Turfgrass Sports Fields. *HortScience* **2016**, *51*, 1176–1183. [CrossRef]
62. Grubbs, R.A.; Straw, C.M.; Bowling, W.J.; Radcliffe, D.E.; Taylor, Z.; Henry, G.M. Predicting Spatial Structure of Soil Physical and Chemical Properties of Golf Course Fairways Using an Apparent Electrical Conductivity Sensor. *Precis. Agric.* **2019**, *20*, 496–519. [CrossRef]
63. Adamchuk, V.I.; Biswas, A.; Huang, H.; Holland, J.E.; Taylor, J.A.; Stenberg, B.; Wetterlind, J.; Minasny, B.; Fidelis, C.; Yinil, D.; et al. Soil Sensing. In *Sensing Approaches for Precision Agriculture*; Kerry, R., Escolà, A., Eds.; Springer Nature: Cham, Switzerland, 2021; p. 415.
64. Kerry, R.; Ingram, B.; Oliver, M.A.; Frogbrook, Z.L. Soil Sampling and Sensed Ancillary Data Requirements for Soil Mapping in Precision Agriculture I. Delineation of Management Zones to Determine Zone Averages of Soil Properties. *Precis. Agric.* **2024**, *25*, 1181–1211. [CrossRef]
65. Kerry, R.; Ingram, B.; Oliver, M.A.; Frogbrook, Z.L. Soil Sampling and Sensed Ancillary Data Requirements for Soil Mapping in Precision Agriculture II: Contour Mapping of Soil Properties with Sensed Z-Score Data for Comparison with Management Zone Averages. *Precis. Agric.* **2024**, *25*, 1212–1234. [CrossRef]
66. Kerry, R.; Ingram, B.; Sanders, K.; Hammond, K.; Hansen, N.; Jensen, R.; Hopkins, B. Assessing the Ability of ECa and Drone Data to Capture Spatial Patterns in Soil Moisture for More Precise Turfgrass Irrigation. In Proceedings of the 14th European Conference on Precision Agriculture'23, Bologna, Italy, 2–6 July 2023. [CrossRef]
67. Burgin, H.R.; Wear, G.A.; Hansen, N.C.; Hopkins, B.G. Variable Impacts on Growth of Deficit Irrigation on *Cynodon dactylon* (L.) Pers. × Cynodon transvaalensis Burtt Davy and *Poa pratensis* L. *Int. Turfgrass Soc. Res. J.* **2022**, *14*, 152–156. [CrossRef]
68. Heil, K.; Schmidhalter, U. The Application of EM38: Determination of Soil Parameters, Selection of Soil Sampling Points and Use in Agriculture and Archaeology. *Sensors* **2017**, *17*, 2540. [CrossRef]
69. Gitelson, A.A.; Kaufman, Y.J.; Stark, R.; Rundquist, D. Novel Algorithms for Remote Estimation of Vegetation Fraction. *Remote Sens. Environ.* **2002**, *80*, 76–87. [CrossRef]
70. Jacquez, G.M.; Goovaerts, P.; Kaufmann, A.; Rommel, R. *SpaceStat 4.0 User Manual: Software for the Space-Time Analysis of Dynamic Complex Systems*, 4th ed.; BioMedware: Ann Arbor, MI, USA, 2014.
71. IBM Corp. *IBM SPSS Statistics for Windows*; Version 28.0; IBM Corp: Armonk, NY, USA, 2021.
72. Rogerson, P.A. *Statistical Methods for Geography. A Student's Guide*, 5th ed.; Sage: London, UK, 2020; p. 405.
73. Kerry, R.; Oliver, M.A. Variograms of ancillary data to aid sampling for soil surveys. *Precis. Agric.* **2003**, *4*, 261–278. [CrossRef]
74. Rahman, M.M.; McDermid, G.J.; McKeeman, T.; Lovitt, J. A Workflow to Minimize Shadows in UAV-Based Orthomosaics. *J. Unmanned Veh. Syst.* **2019**, *7*, 2. [CrossRef]
75. UN. The Sustainable Development Goals Report. 2020. Available online: https://unstats.un.org/sdgs/report/2020/ (accessed on 31 May 2024).